Acta Mech 226, 3881–3904 (2015)
DOI 10.1007/s00707-015-1435-y

ORIGINAL PAPER

Lin Chen

Green's function for a transversely isotropic multi-layered half-space: an application of the precise integration method

Received: 26 September 2014 / Revised: 26 June 2015 / Published online: 11 August 2015

Abstract A numerical approach is presented for the evaluation of Green's function for a multi-layered half-space. The formulation is unconditionally stable and has the computational simplicity with only the algebraic calculations involved. It imposes no limit to the thickness of the layered medium and the magnitude of frequency. In the analysis, the Fourier–Bessel transform and precise integration method (PIM) are employed. Here, the Fourier–Bessel transform is employed to convert the wave motion equation from the spatial domain to the wavenumber domain, which derives a second-order ordinary differential equation. Then, a dual vector representation of wave motion equation is introduced to reduce the second-order differential equation to first order. It is solved by PIM. Finally, the Green's function in the wavenumber domain is obtained. In order to calculate the Green's function in the spatial domain, the inverse Fourier–Bessel transform over the wavenumber is employed for deriving the solutions, which results in a one-dimensional infinite integral with Bessel functions involved. An adaptive Gauss quadrature is used for the evaluation of this integral. Numerical examples are provided to demonstrate the capability of the proposed method. Comparisons with other methods are made. Very promising results are obtained.

1 Introduction

A large number of experiments indicate that the soil medium in nature always exhibits some degree of anisotropy in its response to stress. For instance, the natural clay deposits, during the physical process of their formation, will make the particles or particle-units orient in a horizontal arrangement. Due to this preferred orientation and the resulting electrochemical bonds among the clay particles, the soil medium is always horizontally layered and exhibits the transversely isotropic property, as demonstrated in the experiments [1–3]. Thus, in this paper, an elastic problem for a transversely isotropic medium is relevant.

The Green's function for a multi-layered medium is significant in applied mechanics and civil engineering since it yields the best description of the dynamic properties of the medium. It is a subject of fundamental interest because of its relevance to soil dynamics, soil–structure interaction, earthquake engineering, seismology and geophysical methods [4–6]. Considering this, the Green's function for the transversely isotropic medium is concerned in the paper. Starting from the well-known work of Stoneley [7], a large number of studies have been carried out for the transversely isotropic medium on the basis of wave propagation theory. Here, for brevity, only a few significant ones are presented for reference. By applying the Fourier expansion and integral transforms, Anderson [8], Buchwald [9], Singh [10], Seale et al. [11], Rajapakse et al. [12], Wang et al. [13] obtained the analytical solutions for the surface displacements (Green's function) of a transversely isotropic

L. Chen (✉)
Lehrstuhl für Baustatik und Baudynamik, RWTH Aachen University, Mies-van-der-Rohe-Str. 1, 52074 Aachen, Germany
E-mail: lin.chen@lbb.rwth-aachen.de

half-space. Additionally, on the basis of the potential method, Wang et al. [14], Shodja et al. [15] and Rahimian et al. [16] presented the analytical solution of the Green's function for a homogenous transversely isotropic medium subjected to time-harmonic excitations. Although the considerable analytical solutions are available now, they are still restricted to a relatively simple medium, such as a full-space or half-space. The corresponding analytical solutions for a multi-layered medium with arbitrary boundary conditions do not exist, because the integral formulations need to be evaluated numerically. Among these works, one could firstly mention the detailed reviews by Pao [17] and Nayfeh [18] on this subject. In their works, the major research contributions for the analysis of elastic waves in the multi-layered medium were presented. By applying the Cagniard–de Hoop method, van der Hijden [19] solved the differential equation of wave motion in the layered medium and obtained the dynamic response (Green's function) in the medium. Tan [20,21] employed the reflection matrix method to calculate the Green's function for an arbitrarily thick multi-layered medium. Pan et al. [22,23] employed the propagation matrix method to calculate the three-dimensional Green's function for a transversely isotropic multi-layered half-space. Based on the potential method, Khojasteh et al. [24,25] presented an efficient derivation of the Green's function for a transversely isotropic multi-layered medium. Additionally, by employing the thin-layer method (TLM), Waas et al. [26], Kausel [27] and Oliveira and Kausel [28] obtained the numerical representation of the dynamic response (Green's function) of a transversely isotropic multi-layered half-space.

In this paper, a numerical approach to calculate the Green's function for a transversely isotropic multi-layered half-space is presented. The development of the method is guided by the desire to accomplish the following objectives, and it should be:

1. valid for the wide range of frequency interested in seismology and earthquake engineering. There should be no constraint on the magnitude of frequency.
2. suitable for the dynamic analysis of an arbitrarily layered medium. There should be no limitation on the number of layers.
3. stable for models involving solid layers of thicknesses ranging from large values to thin ones. There should be no restriction on the layer thickness.
4. capable of simultaneously calculating the response at several points.

To meet these objectives, the Fourier–Bessel transform and precise integration method (PIM) [29] are employed. PIM is an efficient and accurate numerical method for the solution of a one-order ordinary differential equation, which is widely employed in the field of structural dynamics [30–32] and wave propagation analysis [33,34]. In the field of soil–structure interaction analysis, Lin et al. [35–38] applied the precise integration method (PIM) to calculate the displacement Green's function. However, in these works, they can only calculate the displacement Green's function on the top surface of the multi-layered medium. Also, in performing the infinite integrals of the Green's function, they employed the pth-order quasi discrete Hankel transform which exhibits problems connected with the Gibbs phenomenon [39,40]. Recently, to analyze the dynamic response of embedded foundation, Han et al. [41] utilized the precise integration method and stiffness matrix method [42] to calculate the displacement Green's function in the interior of the multi-layered medium. In the analysis, they employed the precise integration method to obtain the stiffness matrix of the layered medium and then used the stiffness matrix method [42] to calculate the displacement response. However, for the stiffness matrix method, it exhibits computational instability as the layer thickness tends to be a small value, which is proved in Sect. 2.3 in this paper and can also be easily proved from the formulations provided in the book of Kausel [42]. Hence, their approach will lead to unstable solutions for the case of small layer thickness.

In this paper, the Green's function (displacement and stress) at any point of the multi-layered medium (on the top surface or inside the medium) will be calculated. The proposed algorithm is proved to be explicit and unconditionally stable. It imposes no limit on the thickness of the layers or the magnitude of frequency. In the implementation, the Fourier–Bessel transform is used to convert the differential equation of wave motion from spatial domain to wavenumber domain. Then, a second-order ordinary differential equation is observed. The dual vector representation of wave motion equation is introduced to reduce the second-order differential equation to first order, which is solved by the precise integration method (PIM). Finally, it obtains the Green's function in the wavenumber domain. For the calculation of the Green's function in the spatial domain, the inverse Fourier–Bessel transform over the wavenumber is employed. An infinite integral involving Bessel functions is derived. It is integrated by an adaptive Gauss quadrature, which is proved to be accurate because a combined relative–absolute error criterion is employed in the calculation [43,44]. Numerical examples are provided in the last part of the paper. The accuracy of the proposed approach is validated by comparison with the Green's function (displacement and stress) of a multi-layered half-space available in the literature [11,25,45].

The advantages of the proposed algorithm are: (a) it overcomes the exponential overflow and computational instability generally encountered with employing the propagation matrix method and transfer matrix method; (b) it avoids the huge matrix calculation in the thin-layer method; (c) it imposes no limit to the thickness of the layered medium and the magnitude of frequency; (d) it obviates the computational instability in the stiffness matrix method as the layer thickness tends to be a small value.

The paper is organized as follows:

In Sect. 2, the wave motion equation of transversely isotropic medium is derived. Application of the Fourier–Bessel transform to convert the wave motion equation from the spatial domain to the wavenumber domain is addressed. Employment of the precise integration method (PIM) to solve the differential equation is illustrated.

In Sect. 3, the Green's function in the wavenumber domain is obtained. Comparison with the analytical solution is made to validate the theory.

In Sect. 4, the Green's function in the spatial domain by the double-inverse Fourier–Bessel transform is obtained. A one-dimensional infinite integral involving Bessel functions is derived. The calculation of the Green's function under vertical load is addressed for illustration.

In Sect. 5, employment of the adaptive Gauss quadrature to perform the one-dimensional infinite integral is addressed.

In Sect. 6, four numerical examples are presented. The first three examples are used to validate the proposed approach. The last one is employed to demonstrate the capability of the approach.

Conclusions are stated in Sect. 7.

2 Wave propagation in the multi-layered medium

Consider a homogeneous, transversely isotropic half-space overlaid by n parallel layers of a similar medium but with distinct material properties, as shown in Fig. 1. With a cylindrical coordinate system set at the top free surface, the jth layer is characterized by the following material parameters: mass density ρ_j (kg/m^3), Young's moduli E_j (N/m^2) and E'_j (N/m^2), Poisson's ratios ν_j and ν'_j, shear modulus G'_j (N/m^2), material damping ratios ξ_j and ξ'_j and the thickness $h_j = z_j - z_{j-1}$ (m), where z_j and z_{j-1} are the depths of its upper and lower interface, respectively. Here, the units of the variables are given in the brackets. Apparently, if one sets the Young's moduli $E_j = E'_j$, shear modulus $G'_j = E_j/2\left(1+\nu_j\right)$, Poisson's ratios $\nu_j = \nu'_j$ and material damping ratios $\xi_j = \xi'_j$, an isotropic soil layer is observed. The material parameters of the half-space are denoted as ρ_H, E_H and E'_H, ν_H and ν'_H, G'_H, ξ_H and ξ'_H. Here, the constants without prime refer to the quantities in the plane of transverse isotropy, while the constants with prime refer to the quantity in the plane normal to the plane of transverse isotropy. The medium is subjected to an arbitrarily distributed force (on the plane $z = z_s$), which is located in the kth layer and centered on the vertical axis, as shown in Fig. 1. It can be represented as a set of prescribed stress discontinuities across the corresponding planar region.

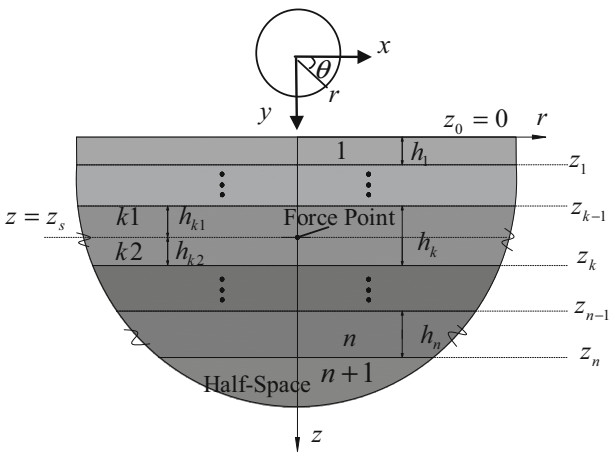

Fig. 1 Multi-layered half-space with internal source

2.1 Transformation of the wave motion equation

In the cylindrical coordinate system, the stress–strain relation for a transversely isotropic medium is

$$\boldsymbol{\sigma} = \begin{bmatrix} \sigma_{rr} \\ \sigma_{\theta\theta} \\ \sigma_{zz} \\ \tau_{\theta z} \\ \tau_{rz} \\ \tau_{r\theta} \end{bmatrix} = C\boldsymbol{\varepsilon} = \begin{bmatrix} d_{11} & d_{11}-2d_{66} & d_{13} & 0 & 0 & 0 \\ d_{11}-2d_{66} & d_{11} & d_{13} & 0 & 0 & 0 \\ d_{13} & d_{13} & d_{33} & 0 & 0 & 0 \\ 0 & 0 & 0 & d_{44} & 0 & 0 \\ 0 & 0 & 0 & 0 & d_{44} & 0 \\ 0 & 0 & 0 & 0 & 0 & d_{66} \end{bmatrix} \begin{bmatrix} \varepsilon_{rr} \\ \varepsilon_{\theta\theta} \\ \varepsilon_{zz} \\ \varepsilon_{\theta z} \\ \varepsilon_{rz} \\ \varepsilon_{r\theta} \end{bmatrix} \tag{1}$$

where d_{ij} $(i, j = 1, 2, \ldots, 6)$ are the elastic constants of the medium and can be expressed in terms of the material parameters of the soil medium (engineering constants):

$$\begin{aligned} d_{11} &= \frac{E\left(1-\left(E/E'\right)\nu'^2\right)}{(1+\nu)\left(1-\nu-(2E/E')\,\nu'^2\right)}, \quad d_{13} = \frac{E\nu'}{1-\nu-(2E/E')\,\nu'^2}, \\ d_{33} &= \frac{E'(1-\nu)}{1-\nu-(2E/E')\,\nu'^2}, \quad d_{44} = G', \quad d_{66} = \frac{E}{2(1+\nu)}. \end{aligned} \tag{2}$$

If the internal material damping is considered, one needs to replace E, E' and G' by the complex Young's moduli and shear modulus, i.e., $E(1+2\xi i)$, $E'\left(1+2\xi' i\right)$ and $G'\left(1+2\xi' i\right)$, where ξ and ξ' are the damping ratios, $i = \sqrt{-1}$. In addition, in defining the material properties, the positive strain energy should be unconditionally satisfied. Thus, the following constraints for the material constants d_{ij} should hold [25]:

$$(d_{11}-d_{66})\,d_{33} > d_{13}^2, \quad d_{44} > 0, \quad d_{66} > 0. \tag{3}$$

For analytical and numerical purposes, it is beneficial to introduce the dimensionless parameters for the kth layer $(k = 1, 2, \ldots, n, n+1)$, which will be employed in the numerical examples,

$$\bar{\rho}_k = \rho_k/\rho_0, \quad \bar{E}_k = E_k/d_{66}^0, \quad \bar{E}'_k = E'_k/d_{66}^0, \quad \bar{G}'_k = G'_k/d_{66}^0, \quad \bar{d}_{ij}^k = d_{ij}/d_{66}^0, \tag{4}$$

in which ρ_0 and d_{66}^0 are the reference mass density and elastic constant, respectively. Also, it defines a reference wavenumber $a_0 = \omega\sqrt{\rho_0/d_{66}^0}$ to normalize the frequency.

In the cylindrical coordinate system, the general differential equations of wave motion are

$$\begin{aligned} &\frac{\partial\sigma_{rr}}{\partial r} + \frac{1}{r}\frac{\partial\tau_{\theta r}}{\partial\theta} + \frac{\partial\tau_{zr}}{\partial z} + \frac{\sigma_{rr}-\sigma_{\theta\theta}}{r} = \rho\frac{\partial^2 u_r}{\partial t^2}, \\ &\frac{\partial\tau_{r\theta}}{\partial r} + \frac{1}{r}\frac{\partial\sigma_{\theta\theta}}{\partial\theta} + \frac{\partial\tau_{z\theta}}{\partial z} + \frac{2\tau_{r\theta}}{r} = \rho\frac{\partial^2 u_\theta}{\partial t^2}, \quad \frac{\partial\tau_{rz}}{\partial r} + \frac{1}{r}\frac{\partial\tau_{\theta z}}{\partial\theta} + \frac{\partial\sigma_{zz}}{\partial z} + \frac{\tau_{rz}}{r} = \rho\frac{\partial^2 u_z}{\partial t^2}, \end{aligned} \tag{5}$$

where u_r, u_θ and u_z are the radial, tangential and vertical displacements, respectively. The problem is solved in the frequency domain. The variation with time is given by the factor $e^{\mathrm{i}\omega t}$.

In the cylindrical coordinate system, the strain–displacement relations are

$$\begin{aligned} &\varepsilon_r = \frac{\partial u_r}{\partial r}, \quad \varepsilon_\theta = \frac{1}{r}\frac{\partial u_\theta}{\partial\theta} + \frac{u_r}{r}, \quad \varepsilon_z = \frac{\partial u_z}{\partial z}, \\ &\gamma_{\theta z} = \frac{1}{r}\frac{\partial u_z}{\partial\theta} + \frac{\partial u_\theta}{\partial z}, \quad \gamma_{zr} = \frac{\partial u_r}{\partial z} + \frac{\partial u_z}{\partial r}, \quad \gamma_{r\theta} = \frac{\partial u_\theta}{\partial r} + \frac{1}{r}\frac{\partial u_r}{\partial\theta} - \frac{u_\theta}{r}. \end{aligned} \tag{6}$$

The Navier–Cauchy equation for the homogeneous transversely isotropic medium is observed by substituting Eqs. (1) and (6) in Eq. (5),

$$\left[d_{11}\left(\frac{\partial^2}{\partial r^2}+\frac{1}{r}\frac{\partial}{\partial r}-\frac{1}{r^2}\right)+\frac{d_{66}}{r^2}\frac{\partial^2}{\partial\theta^2}+d_{44}\frac{\partial^2}{\partial z^2}\right]u_r+\left[\frac{(d_{11}-d_{66})}{r}\frac{\partial^2}{\partial r\partial\theta}-\frac{(d_{11}+d_{66})}{r^2}\frac{\partial}{\partial\theta}\right]u_\theta$$
$$+(d_{13}+d_{44})\frac{\partial^2 u_z}{\partial r\partial z}+\rho\omega^2 u_r=0$$
$$\left[\frac{(d_{11}-d_{66})}{r}\frac{\partial^2}{\partial r\partial\theta}+\frac{(d_{11}+d_{66})}{r^2}\frac{\partial}{\partial\theta}\right]u_r+\left[d_{66}\left(\frac{\partial^2}{\partial r^2}+\frac{1}{r}\frac{\partial}{\partial r}-\frac{1}{r^2}\right)+\frac{d_{11}}{r^2}\frac{\partial^2}{\partial\theta^2}+d_{44}\frac{\partial^2}{\partial z^2}\right]u_\theta$$
$$+\frac{(d_{13}+d_{44})}{r}\frac{\partial^2 u_z}{\partial\theta\partial z}+\rho\omega^2 u_\theta=0$$
$$(d_{13}+d_{44})\left(\frac{\partial^2}{\partial r\partial z}+\frac{1}{r}\frac{\partial}{\partial z}\right)u_r+\frac{(d_{13}+d_{44})}{r}\frac{\partial^2 u_\theta}{\partial\theta\partial z}$$
$$+\left[d_{44}\left(\frac{\partial^2}{\partial r^2}+\frac{1}{r}\frac{\partial}{\partial r}+\frac{1}{r^2}\frac{\partial^2}{\partial\theta^2}\right)+d_{33}\frac{\partial^2}{\partial z^2}\right]u_z+\rho\omega^2 u_z=0. \tag{7}$$

Since the material is transversely isotropic, the wave motion equation can be decoupled into in-plane wave motion (P–SV wave) and out-of-plane wave motion (SH wave) in the transformed wavenumber domain. The transformations are performed by the Fourier–Bessel transform [42]

$$\mathbf{U}(r,\theta,z)=\sum_{n=0}^{\infty}\mathbf{T}(n\theta)\int_{k=0}^{\infty}k\mathbf{C}_n(kr)\bar{\mathbf{U}}(k,z,n)\mathrm{d}k,$$
$$\bar{\mathbf{U}}(k,z,n)=a_n\int_{r=0}^{\infty}r\mathbf{C}_n(kr)\int_{\theta=0}^{2\pi}\mathbf{T}(n\theta)\mathbf{U}(r,\theta,z)\mathrm{d}r\mathrm{d}\theta \tag{8}$$

where $\bar{\mathbf{U}}(k,z)=\{\bar{u}_r,\bar{u}_\theta,\bar{u}_z\}^{\mathrm{T}}$ denotes the displacement vector in the wavenumber domain. The superscript bar is a reminder that the components are defined in the wavenumber domain. $\mathbf{U}(r,\theta,z)=(u_r,u_\theta,u_z)^{\mathrm{T}}$ refers to the displacement in the spatial domain.

The orthogonalization factor a_n is the normalization factor, which is equal to $1/2\pi$ for $n=0$ and $1/\pi$ for $n\neq 0$. The diagonal matrix $\mathbf{T}(n\theta)$ is $\mathbf{T}(n\theta)=\mathrm{diag}[\cos n\theta,-\sin n\theta,\cos n\theta]$ for the symmetric case about the x axis (the r axis at $\theta=0$); and $\mathbf{T}(n\theta)=\mathrm{diag}[\sin n\theta,\cos n\theta,\sin n\theta]$ for the anti-symmetric case. θ is the angle of revolution around the x axis. The matrix $\mathbf{C}_n(kr)$ includes Bessel functions, which is

$$\mathbf{C}_n(kr)=\begin{bmatrix}\frac{\mathrm{d}J_n(kr)}{\mathrm{d}(kr)} & \frac{nJ_n(kr)}{kr} & 0\\ \frac{nJ_n(kr)}{kr} & \frac{\mathrm{d}J_n(kr)}{\mathrm{d}(kr)} & 0\\ 0 & 0 & -J_n(kr)\end{bmatrix} \tag{9}$$

in which $J_n(kr)$ is the first kind Bessel function with nth order.

For the evaluation of Green's function, only the cases of $n=0$ and $n=1$ in Eq. (8) need to be considered; see [46]. The $n=0$ corresponds to an axisymmetric load case (such as uniformly distributed vertical or torsional load on a disk), while the $n=1$ is used to the load case which is symmetric about the x axis (such as uniformly distributed horizontal or rocking load on a disk).

Similar domain transformations can be performed for the stress vector $\mathbf{P}(r,\theta,z)$ as Eq. (8) via substituting the displacement vector with the stress vector. The definitions of the stress vector in the spatial domain and wavenumber domain are

$$\mathbf{P}(r,\theta,z)=\{\tau_{rz},\tau_{\theta z},\sigma_{zz}\}^{\mathrm{T}},\quad \bar{\mathbf{P}}(k,z)=\{\bar{\tau}_{rz},\bar{\tau}_{\theta z},\bar{\sigma}_{zz}\}^{\mathrm{T}}. \tag{10}$$

By executing the Fourier–Bessel transform of Eq. (7), it will obtain the in-plane wave motion equation and out-of-plane wave motion equation. In-plane wave motion relates to the displacements $\bar{u}_r(k,z)$ and $\bar{u}_z(k,z)$. The corresponding equations are

$$\begin{cases}d_{44}\bar{u}_r''(k,z)-ik(d_{13}+d_{44})\bar{u}_z'(k,z)-\left(d_{11}k^2-\rho\omega^2\right)\bar{u}_r(k,z)=0\\ d_{33}\bar{u}_z''(k,z)-ik(d_{13}+d_{44})\bar{u}_r'(k,z)-\left(d_{44}k^2-\rho\omega^2\right)\bar{u}_z(k,z)=0.\end{cases} \tag{11}$$

Out-of-plane wave motion is related to the displacement $\bar{u}_\theta(k,z)$ by

$$d_{44}\bar{u}_\theta''(k,z) - \left(d_{66}k^2 - \rho\omega^2\right)\bar{u}_\theta(k,z) = 0. \tag{12}$$

In Eqs. (11) and (12), $(\cdot)' = \partial(\cdot)/\partial z$. It is worthwhile to note that the displacements are identical for every point at the same elevation z in the wavenumber domain [28]. Hence, in the following, we do not mention the displacement of which point is calculated, but only the elevation of the point.

The wave motion equations in Eqs. (11) and (12) can be written in a matrix form

$$\mathbf{K}_{22}\bar{\mathbf{U}}'' + (\mathbf{K}_{21} - \mathbf{K}_{12})\bar{\mathbf{U}}' - \left(\mathbf{K}_{11} - \rho\omega^2\mathbf{I}\right)\bar{\mathbf{U}} = 0 \tag{13}$$

where $\bar{\mathbf{U}}$ is the displacement vector in the wavenumber domain; see Eq. (8); $\mathbf{I}$ is a 3×3 unit matrix. The coefficient matrices are

$$\mathbf{K}_{11} = k^2\begin{bmatrix} d_{11} & 0 & 0 \\ 0 & d_{66} & 0 \\ 0 & 0 & d_{44} \end{bmatrix}, \quad \mathbf{K}_{12} = \mathbf{K}_{21}^H = ik\begin{bmatrix} 0 & 0 & d_{13} \\ 0 & 0 & 0 \\ d_{44} & 0 & 0 \end{bmatrix}, \quad \mathbf{K}_{22} = \begin{bmatrix} d_{44} & 0 & 0 \\ 0 & d_{44} & 0 \\ 0 & 0 & d_{33} \end{bmatrix} \tag{14}$$

in which the superscript H denotes the Hermitian transpose.

From the constitutive relations, the stress vector $\bar{\mathbf{P}}$ in Eq. (10) satisfies

$$\bar{\mathbf{P}} = \left(\mathbf{K}_{22}\bar{\mathbf{U}}' + \mathbf{K}_{21}\bar{\mathbf{U}}\right). \tag{15}$$

Substituting Eq. (15) in Eq. (13), it can be written as the following dual vector representation of wave motion equation:

$$\bar{\mathbf{V}}' = \begin{Bmatrix} \bar{\mathbf{U}} \\ \bar{\mathbf{P}} \end{Bmatrix}' = \mathbf{\Pi}\bar{\mathbf{V}} = \begin{bmatrix} \mathbf{A} & \mathbf{D} \\ \mathbf{B} & \mathbf{C} \end{bmatrix}\begin{Bmatrix} \bar{\mathbf{U}} \\ \bar{\mathbf{P}} \end{Bmatrix}. \tag{16}$$

in which

$$\mathbf{A} = -\mathbf{K}_{22}^{-1}\mathbf{K}_{21} = -\mathbf{C}^H, \quad \mathbf{B} = \mathbf{K}_{11} - \mathbf{K}_{12}\mathbf{K}_{22}^{-1}\mathbf{K}_{21} - \rho\omega^2\mathbf{I}, \quad \mathbf{D} = \mathbf{K}_{22}^{-1}. \tag{17}$$

The continuity conditions at the interface between two layers are

$$\bar{\mathbf{U}}_i^+ = \bar{\mathbf{U}}_i^-, \quad \bar{\mathbf{P}}_i^+ = \bar{\mathbf{P}}_i^-, \quad (i = 1, 2, \ldots, n-1, n). \tag{18}$$

2.2 Wave motion in the half-space

Two cases of a layered half-space are considered: the layered medium on a rigid base and on a semi-infinite space. In the former case, there is no displacement at the bottom plane $z = z_n$,

$$\bar{\mathbf{U}} = \mathbf{0}, \quad (z = z_n). \tag{19}$$

In the latter case, the radiation conditions should be considered. The state equation Eq. (16) for the semi-infinite space, i.e., the $(n+1)$ th layer, is expressed as

$$\bar{\mathbf{V}}'_{n+1} = \mathbf{\Pi}_{n+1}\bar{\mathbf{V}}_{n+1}. \tag{20}$$

Then, the eigenvalue equation of $\mathbf{\Pi}_{n+1}$ is solved:

$$\mathbf{\Pi}_{n+1}\bar{\mathbf{T}}_{n+1} = \bar{\mathbf{T}}_{n+1}\bar{\mathbf{\Lambda}}_{n+1} \tag{21}$$

where $\bar{\mathbf{\Lambda}}_{n+1}$ and $\bar{\mathbf{T}}_{n+1}$ are the eigenvalues and eigenvectors of matrix $\mathbf{\Pi}_{n+1}$, partitioned as

$$\bar{\mathbf{\Lambda}}_{n+1} = \begin{bmatrix} \mathbf{\lambda}_p & 0 \\ 0 & \mathbf{\lambda}_n \end{bmatrix}, \quad \bar{\mathbf{T}}_{n+1} = \begin{bmatrix} \bar{\mathbf{T}}_{u1} & \bar{\mathbf{T}}_{u2} \\ \bar{\mathbf{T}}_{q1} & \bar{\mathbf{T}}_{q2} \end{bmatrix}. \tag{22}$$

The real part of all terms of $\mathbf{\lambda}_p$ is positive (subscript 'p' for positive) and of $\mathbf{\lambda}_n = -\mathbf{\lambda}_p$ negative (subscript 'n' for negative). The solution of Eq. (20) equals

$$\bar{\mathbf{V}}_{n+1} = \begin{bmatrix} \bar{\mathbf{T}}_{u1} & \bar{\mathbf{T}}_{u2} \\ \bar{\mathbf{T}}_{q1} & \bar{\mathbf{T}}_{q2} \end{bmatrix}\begin{bmatrix} \exp\left(\mathbf{\lambda}_p(z - z_n)\right) & 0 \\ 0 & \exp\left(\mathbf{\lambda}_n(z - z_n)\right) \end{bmatrix}\begin{Bmatrix} \mathbf{c}_1 \\ \mathbf{c}_2 \end{Bmatrix}. \tag{23}$$

Expending Eq. (23) yields the displacement and stress in the semi-infinite space ($z \geq z_n$)

$$\begin{aligned}\bar{\mathbf{U}} &= \bar{\mathbf{T}}_{u1} \exp\left(\boldsymbol{\lambda}_p (z - z_n)\right) \mathbf{c}_1 + \bar{\mathbf{T}}_{u2} \exp\left(\boldsymbol{\lambda}_n (z - z_n)\right) \mathbf{c}_2, \\ \bar{\mathbf{P}} &= \bar{\mathbf{T}}_{q1} \exp\left(\boldsymbol{\lambda}_p (z - z_n)\right) \mathbf{c}_1 + \bar{\mathbf{T}}_{q2} \exp\left(\boldsymbol{\lambda}_n (z - z_n)\right) \mathbf{c}_2.\end{aligned} \tag{24}$$

For the semi-infinite space, the radiation conditions correspond to no upward wave in the space, which leads to $\mathbf{c}_1 = 0$ in Eq. (24). Then, the stress–displacement relation on the plane $z = z_n$ (upper surface of the semi-infinite space) is obtained from eliminating $\mathbf{c}_2$ in Eq. (24),

$$\bar{\mathbf{P}}(z_n) = \bar{\mathbf{T}}_{q2} \bar{\mathbf{T}}_{u2}^{-1} \bar{\mathbf{U}}(z_n) = \bar{\mathbf{R}}_\infty \bar{\mathbf{U}}(z_n). \tag{25}$$

Equation (25) is the general stress–displacement relation for the semi-infinite space. Considering different values of wavenumber k and frequency ω, the following specific equations for $\bar{\mathbf{R}}_\infty$ can be obtained:

(a) Nonzero frequency, nonzero wavenumber: $k > 0, \omega > 0$:

$$\bar{\mathbf{R}}_\infty = \begin{bmatrix} \frac{d_{44}(p_1 b_2 - p_2 b_1)}{b_2 - b_1} & 0 & \frac{i d_{44}(k(b_1 - b_2) + i(p_1 - p_2))}{b_2 - b_1} \\ 0 & \sqrt{d_{44}\left(d_{66}k^2 - \rho_H \omega^2\right)} & 0 \\ \frac{i d_{44}(k(b_2 - b_1) + i(p_2 - p_1))}{b_2 - b_1} & 0 & \frac{d_{33}(p_2 b_2 - p_1 b_1)}{b_2 - b_1} \end{bmatrix} \tag{26}$$

in which

$$p_j = \sqrt{\frac{-m \pm \sqrt{m^2 - 4nl}}{2l}}, \quad b_j = i \frac{k^2 d_{11} - \rho_H \omega^2 - d_{44} p_j^2}{k p_j (d_{13} + d_{44})} \quad (j = 1, 2) \tag{27}$$

where $l = d_{44} d_{33}, m = \left[(d_{13} + d_{44})^2 - \left(d_{11} d_{33} + d_{44}^2\right)\right] k^2 + \rho_H \omega^2 (d_{44} + d_{33}), n = \left(k^2 d_{11} - \rho_H \omega^2\right) \left(k^2 d_{44} - \rho_H \omega^2\right)$.

(b) Zero frequency, nonzero wavenumber: $k > 0, \omega = 0$:

$$\bar{\mathbf{R}}_\infty = \begin{bmatrix} \frac{d_{44}(p_1 b_2 - p_2 b_1)}{b_2 - b_1} & 0 & \frac{i d_{44}(k(b_1 - b_2) + i(p_1 - p_2))}{b_2 - b_1} \\ 0 & \sqrt{d_{44}\left(d_{66}k^2 - \rho_H \omega^2\right)} & 0 \\ \frac{i d_{44}(k(b_2 - b_1) + i(p_2 - p_1))}{b_2 - b_1} & 0 & \frac{d_{33}(p_2 b_2 - p_1 b_1)}{b_2 - b_1} \end{bmatrix} \tag{28}$$

in which

$$p_j = k f_j, \quad b_j = \frac{i}{f_j} \frac{\left(d_{11} - f_j^2 d_{44}\right)}{(d_{13} + d_{44})}, \quad (j = 1, 2) \tag{29}$$

where $f_j = \sqrt{\left\{d_{11} d_{33} + d_{44}^2 - (d_{13} + d_{44})^2 \pm \sqrt{\left(d_{11} d_{33} - d_{44}^2\right)^2 + \left[(d_{13} + d_{44})^2 - 2\left(d_{11} d_{33} + d_{44}^2\right)\right](d_{13} + d_{44})^2}\right\} / 2 d_{44} d_{33}}$.

(c) Nonzero frequency, zero wavenumber: $k = 0, \omega > 0$:

$$\bar{\mathbf{R}}_\infty = \operatorname{diag}\left[i\omega\sqrt{\rho_H d_{44}} \quad i\omega\sqrt{\rho_H d_{44}} \quad i\omega\sqrt{\rho_H d_{33}} \right]. \tag{30}$$

(d) Zero frequency, zero wavenumber: $k = 0, \omega = 0$:

$$\bar{\mathbf{R}}_\infty = \operatorname{diag}\left[0 \quad 0 \quad 0 \right]. \tag{31}$$

2.3 Solution procedure for the multi-layered medium

Within an arbitrary layer, select an interval $[z_a, z_b]$ $(z_a < z_b)$, and assume that it is subjected to external dynamic tractions, $\bar{\mathbf{S}}_a$ and $\bar{\mathbf{S}}_b$, at its upper and lower interfaces, respectively. Hence, if $\bar{\mathbf{U}}_a$ and $\bar{\mathbf{U}}_b$ are the displacement at the two interfaces of the layer, respectively, then

$$\begin{Bmatrix} \bar{\mathbf{S}}_a \\ \bar{\mathbf{S}}_b \end{Bmatrix} = \mathbf{L} \begin{Bmatrix} \bar{\mathbf{U}}_a \\ \bar{\mathbf{U}}_b \end{Bmatrix} = \begin{bmatrix} \mathbf{L}_{aa} & \mathbf{L}_{ab} \\ \mathbf{L}_{ba} & \mathbf{L}_{bb} \end{bmatrix} \begin{Bmatrix} \bar{\mathbf{U}}_a \\ \bar{\mathbf{U}}_b \end{Bmatrix} \tag{32}$$

in which $\mathbf{L}$ is the stiffness matrix of the layer [42].

The corresponding internal force vectors $\bar{\mathbf{P}}_a$ and $\bar{\mathbf{P}}_b$ can be obtained from the force equilibrium,

$$\bar{\mathbf{P}}_a = \bar{\mathbf{S}}_a = \mathbf{L}_{aa}\bar{\mathbf{U}}_a + \mathbf{L}_{ab}\bar{\mathbf{U}}_b, \quad \bar{\mathbf{P}}_b = -\bar{\mathbf{S}}_b = -\mathbf{L}_{ba}\bar{\mathbf{U}}_a - \mathbf{L}_{bb}\bar{\mathbf{U}}_b. \tag{33}$$

Solving Eq. (33) yields the following dual vector form of matrix:

$$\begin{Bmatrix} \bar{\mathbf{U}}_b \\ \bar{\mathbf{P}}_a \end{Bmatrix} = \mathbf{H} \begin{Bmatrix} \bar{\mathbf{U}}_a \\ \bar{\mathbf{P}}_b \end{Bmatrix} = \begin{bmatrix} \mathbf{F} & -\mathbf{G} \\ \mathbf{Q} & \mathbf{E} \end{bmatrix} \begin{Bmatrix} \bar{\mathbf{U}}_a \\ \bar{\mathbf{P}}_b \end{Bmatrix} \tag{34}$$

which implies that the stress–displacement at the two interfaces of one layer is linearly correlated. The matrix $\mathbf{H}$ is the dual matrix; $\mathbf{F}$, $\mathbf{G}$, $\mathbf{Q}$ and $\mathbf{E}$ are termed as correlation matrices of the layer, which can be obtained from Eq. (33). Noticing that the matrix $\mathbf{L}$ is unknown, thus, they cannot be obtained explicitly here. It will solve the correlation matrices $\mathbf{F}$, $\mathbf{G}$, $\mathbf{Q}$ and $\mathbf{E}$ by the precise integration method (PIM) [29] in the next parts.

It is worthwhile to note that, as the layer thickness increases, the correlation matrices $\mathbf{F}$ and $\mathbf{E}$ will tend to zero while $\mathbf{G}$ and $\mathbf{Q}$ will remain stable. The interpretations are: When the layer thickness increases, the waves, produced by the excitation source at the layer interface, may almost attenuate before they reach the opposite side of the layer. Also the reflected waves from the opposite side of the layer may scarcely affect the behavior of this interface. As a result, it seems that the dynamic responses at both interfaces of the layer are independent of each other. Such property can also be observed from Fig. 2. As the thickness increases, $\mathbf{F}(1, 1)$ will tend to zero while $\mathbf{Q}(1, 1)$ will lead to a stable value. Here, the correlation matrices of a single layer are employed to investigate the influence of the layer thickness h. The normalized material properties of the layer are used: material density $\bar{\rho} = 1.5$, Young's moduli $\bar{E} = 2.6$ and $\bar{E}' = 3.0$, Poisson's ratios $\nu = 0.3$ and $\nu' = 0.4$, shear modulus $\bar{G}' = 5.0$, material damping ratios $\xi = 0.05$ and $\xi' = 0.05$. The normalized excitation frequency is $a_0 h = \omega h\sqrt{\rho_0/d_{66}^0} = 1$ and wavenumber k.

Considering that the layer thickness h tends to be a sufficiently large value, then Eq. (34) could be simplified as

$$\begin{Bmatrix} \bar{\mathbf{U}}_b \\ \bar{\mathbf{P}}_a \end{Bmatrix} = \mathbf{H} \begin{Bmatrix} \bar{\mathbf{U}}_a \\ \bar{\mathbf{P}}_b \end{Bmatrix} = \begin{bmatrix} \mathbf{0} & -\mathbf{G} \\ \mathbf{Q} & \mathbf{0} \end{bmatrix} \begin{Bmatrix} \bar{\mathbf{U}}_a \\ \bar{\mathbf{P}}_b \end{Bmatrix}. \tag{35}$$

Contrarily, as the layer thickness h approaches to zero, which denotes a thin layer with $h/\lambda \ll 1$ (h is the layer thickness and λ is the wavelength), the stress and displacement at both interfaces of the layer should be

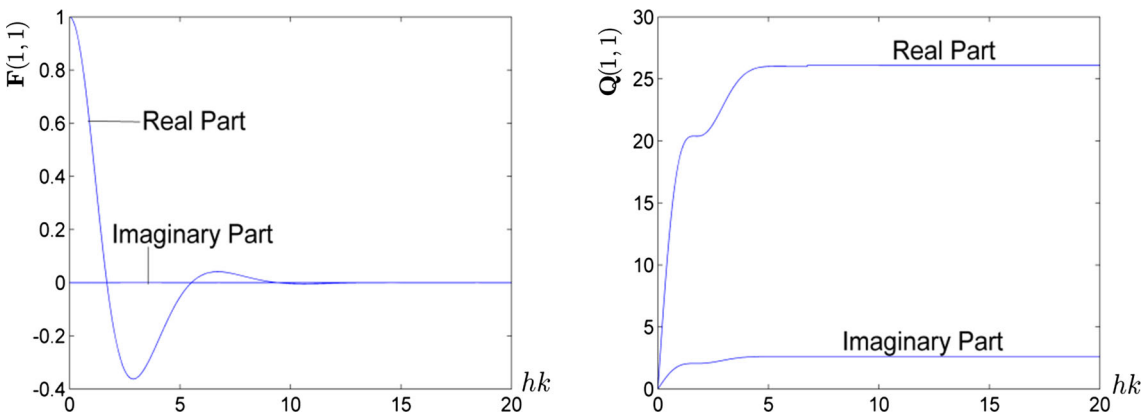

Fig. 2 Property of correlation matrices $\mathbf{F}$ and $\mathbf{Q}$. Here, for brevity, only the terms $\mathbf{F}(1, 1)$ and $\mathbf{Q}(1, 1)$ in the matrices are depicted

almost identical. As a result, the correlation matrices $\mathbf{G}$ and $\mathbf{Q}$ will tend to zero, while $\mathbf{F}$ and $\mathbf{E}$ will lead to unit matrices. Such property can be observed from Fig. 2, as the layer thickness decreases, $\mathbf{F}(1, 1)$ will tend to one while $\mathbf{Q}(1, 1)$ will lead to zero. Considering the extreme case that the layer thickness is zero, it will result in the boundary conditions for the correlation matrices $\mathbf{F}$, $\mathbf{G}$, $\mathbf{Q}$ and $\mathbf{E}$ in Eq. (40).

Currently, for the evaluation of Green's function for a multi-layered medium, the stiffness matrix method [42], the transfer matrix method [47] and the thin-layer method [28] are always employed. The relation between the dual matrix $\mathbf{H}$ and the stiffness matrix $\mathbf{\Lambda}$ in the stiffness matrix method, which relates the displacement and stress at the layer top and bottom, is as below,

$$\begin{Bmatrix} \bar{\mathbf{P}}_a \\ \bar{\mathbf{P}}_b \end{Bmatrix} = \mathbf{\Lambda} \begin{Bmatrix} \bar{\mathbf{U}}_a \\ \bar{\mathbf{U}}_b \end{Bmatrix}, \quad \mathbf{\Lambda} = \begin{bmatrix} \mathbf{Q} + \mathbf{E}\mathbf{G}^{-1}\mathbf{F} & -\mathbf{E}\mathbf{G}^{-1} \\ \mathbf{G}^{-1}\mathbf{F} & -\mathbf{G}^{-1} \end{bmatrix}. \tag{36}$$

Also the transfer matrix $\mathbf{T}$ in the transfer matrix method [47], which relates the stress and displacement scalars ($\bar{\mathbf{U}}$, $\bar{\mathbf{P}}$) at the layer top and bottom, can be represented by the dual matrix $\mathbf{H}$,

$$\begin{Bmatrix} \bar{\mathbf{U}}_b \\ \bar{\mathbf{P}}_b \end{Bmatrix} = \mathbf{T} \begin{Bmatrix} \bar{\mathbf{U}}_a \\ \bar{\mathbf{P}}_a \end{Bmatrix}, \quad \mathbf{T} = \begin{bmatrix} \mathbf{F} + \mathbf{G}\mathbf{E}^{-1}\mathbf{Q} & -\mathbf{G}\mathbf{E}^{-1} \\ -\mathbf{E}^{-1}\mathbf{Q} & \mathbf{E}^{-1} \end{bmatrix}. \tag{37}$$

Generally, the proposed method can directly obtain the stiffness matrix $\mathbf{\Lambda}$ and the transfer matrix $\mathbf{T}$. Additionally, as stated previously, when it increases the layer thickness, only the correlation matrices $\mathbf{G}$ and $\mathbf{Q}$ will remain stable. Consequently, from Eq. (36), the stiffness matrix $\mathbf{\Lambda}$ is always a regular matrix, which is consistent with the analysis of Kausel [42] and Rokhlin et al. [47]. However, the transfer matrix $\mathbf{T}$ in Eq. (37) will become singular; it will exhibit the well-known computational instability problem, which is also in accordance with the analysis of Rokhlin et al. [47]. Conversely, when it decreases the layer thickness to that of a thin layer ($h/\lambda \ll 1$), the correlation matrices $\mathbf{F}$ and $\mathbf{E}$ will tend to be unit matrices, while $\mathbf{G}$ and $\mathbf{Q}$ will lead to zero. Accordingly, the stiffness matrix $\mathbf{\Lambda}$ will become singular, which can also be easily proved from the formulations provided in the book of Kausel [42]. Nevertheless, the transfer matrix $\mathbf{T}$ will remain stable [47]. Thus, the proposed method essentially yields both the merit and demerit of the stiffness matrix method and the transfer matrix method.

Concerning the thin-layer method [28], it is a discrete version of the stiffness matrix method based on the finite element method. It consists of a discretization in the direction of layering into a number of thin sub-layers. The discrete matrices allow finding the normal modes from the solution of a standard eigenvalue problem. However, it is well known that if a physical layer is subdivided into several thin layers, the matrix calculation may be burdened and time-consuming because the dimension of the matrices is proportional to the number of the discretized thin layers. Also, in the calculation, the eigenvalue problem needs to be solved for large matrices. Theoretically, an eigenvalue problem could be solved for any dimension of matrices. However, the current eigenvalue solver is not adequate to solve quite large matrices due to the numerical instability [48], which leads to prohibitive costs and severely taxes the storage memory capabilities of presently available computer hardware.

However, it is worthwhile to note that the proposed method is unconditionally stable, which will be detailedly illustrated in the next parts. In addition, the dimension of all matrices is 3×3, and the computational effort is moderate. It retains the computational simplicity with only the algebraic calculations involved. There is no need to solve the eigenvalue problems. It imposes no limit on the thickness of the layers or the magnitude of frequency. It obviates the singularity problem of the stiffness matrix method when the layer thickness decreases to that of a thin layer ($h/\lambda \ll 1$). Also, it can avoid the computational instability of the transfer matrix method as the layer thickness increases. Employing the adaptive Gauss quadrature in Sect. 5 to calculate the Green's function in the spatial domain, the algorithm is accurate because a combined relative–absolute error criterion is employed to terminate the calculation. If the error criterion is not satisfied, new Gauss points are added. At each step, it retains the integral kernel and Bessel function values so that only the new integrand values need to be calculated. Hence, to achieve a special level of accuracy, one only needs to choose proper relative and absolute errors in the calculation. In the numerical examples, the relative and absolute errors are set as 10^{-6} and 10^{-7}, which is sufficient for the engineering calculation.

Considering any two adjacent layers 1 and 2 ranging in $[z_a, z_b]$ and $[z_b, z_c]$, respectively, now, we apply Eq. (34) to the two layers to merge into a new layer c ranging in $[z_a, z_c]$ with the continuity condition at the interface between them. The corresponding correlation matrices for the newly combined layer c are obtained as

$$\begin{aligned} \mathbf{F}_c &= \mathbf{F}_2 (\mathbf{I} + \mathbf{G}_1\mathbf{Q}_2)^{-1} \mathbf{F}_1, \quad \mathbf{G}_c = \mathbf{G}_2 + \mathbf{F}_2\mathbf{G}_1 (\mathbf{I} + \mathbf{Q}_2\mathbf{G}_1)^{-1} \mathbf{E}_2, \\ \mathbf{Q}_c &= \mathbf{Q}_1 + \mathbf{E}_1\mathbf{Q}_2 (\mathbf{I} + \mathbf{G}_1\mathbf{Q}_2)^{-1} \mathbf{F}_1, \quad \mathbf{E}_c = \mathbf{E}_1 (\mathbf{I} + \mathbf{Q}_2\mathbf{G}_1)^{-1} \mathbf{E}_2 \end{aligned} \tag{38}$$

where the subscripts 1, 2 and c denote the corresponding layer that the correlation matrices belong to. $\mathbf{I}$ denotes a unit matrix. Here, it can be observed that, when it performs the layer combination in Eq. (38), the formulations remain stable no matter whether the layer thickness tends to be that of a thin layer ($h/\lambda \ll 1$) or increases to a large value. It can be interpreted that: in case the layer thickness increases, the formulations involve only the inverse of the stable matrices $\mathbf{G}$ and $\mathbf{Q}$, which correspondingly maintains the computational stability; in case the layer thickness decreases to that of a thin layer, the correlation matrices $\mathbf{F}$ and $\mathbf{E}$ will tend to be unit matrices, while $\mathbf{G}$ and $\mathbf{Q}$ will lead to zero. As a result, all the formulations in Eq. (38) will remain stable.

Since $\bar{\mathbf{U}}_a$ and $\bar{\mathbf{P}}_b$ are mutually independent in Eq. (34), differentiating it with respect to z_b and comparing with Eq. (16), one can obtain a set of ordinary differential equations

$$\mathbf{F}' = (\mathbf{A} + \mathbf{GB})\,\mathbf{F}, \quad \mathbf{G}' = \mathbf{AG} - \mathbf{GC} - \mathbf{D} + \mathbf{GBG}, \quad \mathbf{Q}' = -\mathbf{EBF}, \quad \mathbf{E}' = \mathbf{E}\,(\mathbf{BG} - \mathbf{C})\,. \tag{39}$$

Let z_b approach z_a, the boundary conditions for these equations are derived as

$$\mathbf{E}\,(z_a, z_a) = \mathbf{F}\,(z_a, z_a) = \mathbf{I}, \quad \mathbf{G}\,(z_a, z_a) = \mathbf{Q}\,(z_a, z_a) = \mathbf{0}. \tag{40}$$

Equation (39) shows that the matrices $\mathbf{F}$, $\mathbf{G}$, $\mathbf{Q}$ and $\mathbf{E}$ are coupled with each other. In order to obtain them, the precise integration method (PIM) [29] will be employed. The detailed theoretical derivation of the method can be found in the work of Zhong. Here, only the application of the method in the present study will be addressed.

For an arbitrary ith layer ($i = 1, 2, \ldots, n$) of the layered medium, it assumes the thickness of the layer being h_i. The layer is firstly divided into 2^{N_1} (N_1 is an integer, $N_1 = 6{-}20$) sub-layers of equal thickness $\bar{h}_i = h_i/2^{N_1}$. Then, each sub-layer is further divided into 2^{N_2} (N_2 is an integer, $N_2 = 12{-}20$) mini-layers of equal thickness $\tau = \bar{h}_i/2^{N_2}$. In this paper, $N_1 = 20$ and $N_2 = 20$ are chosen. Under such condition, the thickness of the mini-layers is $\tau = \bar{h}_i/2^{N_2} = h_i/2^{N_1+N_2} = h_i/(1048576 \times 1048576)$. Since the thickness τ is extremely small, the correlation matrices $\mathbf{F}\,(\tau)$, $\mathbf{G}\,(\tau)$, $\mathbf{Q}\,(\tau)$ and $\mathbf{E}\,(\tau)$ can be expressed in terms of Taylor series expansion. Any desired accuracy can be achieved with increasing terms of Taylor expansion. In this paper, four terms of Taylor series are considered. The Taylor series expansion is truncated after the τ^4 terms. Therefore, the relative order of the neglected terms is τ^4. With $N_2 = 20$, τ has been divided by even more than 10^6. Thus, τ^4 will be of the order 10^{-24}, which is well beyond the precision of real*8 typically only the leftmost 15 digits significant. The correlation matrices $\mathbf{F}\,(\tau)$, $\mathbf{G}\,(\tau)$, $\mathbf{Q}\,(\tau)$ and $\mathbf{E}\,(\tau)$ are expressed as

$$\begin{aligned}
&\mathbf{Q}\,(\tau) \approx \boldsymbol{\theta}_1\tau + \boldsymbol{\theta}_2\tau^2 + \boldsymbol{\theta}_3\tau^3 + \boldsymbol{\theta}_4\tau^4, \quad \mathbf{G}\,(\tau) \approx \boldsymbol{\gamma}_1\tau + \boldsymbol{\gamma}_2\tau^2 + \boldsymbol{\gamma}_3\tau^3 + \boldsymbol{\gamma}_4\tau^4,\\
&\tilde{\mathbf{F}}\,(\tau) \approx \mathbf{f}_1\tau + \mathbf{f}_2\tau^2 + \mathbf{f}_3\tau^3 + \mathbf{f}_4\tau^4, \quad \mathbf{F}\,(\tau) = \mathbf{I} + \tilde{\mathbf{F}}\,(\tau),\\
&\tilde{\mathbf{E}}\,(\tau) \approx \boldsymbol{\varphi}_1\tau + \boldsymbol{\varphi}_2\tau^2 + \boldsymbol{\varphi}_3\tau^3 + \boldsymbol{\varphi}_4\tau^4, \quad \mathbf{E}\,(\tau) = \mathbf{I} + \tilde{\mathbf{E}}\,(\tau)
\end{aligned} \tag{41}$$

where $\boldsymbol{\theta}_i, \boldsymbol{\gamma}_i, \mathbf{f}_i$ and $\boldsymbol{\varphi}_i$, $(i = 1, 2, 3, 4)$ are coefficient matrices to be determined. Substituting Eq. (41) in (39), the coefficients of various τ must be equal to zero, which leads to

$$\boldsymbol{\theta}_1 = -\mathbf{B}, \quad \boldsymbol{\gamma}_1 = -\mathbf{D}, \quad \mathbf{f}_1 = \mathbf{A}, \quad \boldsymbol{\varphi}_1 = -\mathbf{C}, \tag{42}$$

$$\boldsymbol{\theta}_2 = -\,(\boldsymbol{\varphi}_1\mathbf{B} + \mathbf{Bf}_1)/2, \quad \boldsymbol{\gamma}_2 = (\mathbf{A}\boldsymbol{\gamma}_1 - \boldsymbol{\gamma}_1\mathbf{C})/2, \quad \mathbf{f}_2 = (\mathbf{Af}_1 + \boldsymbol{\gamma}_1\mathbf{B})/2, \quad \boldsymbol{\varphi}_2 = (\mathbf{B}\boldsymbol{\gamma}_1 - \boldsymbol{\varphi}_1\mathbf{C})/2, \tag{43}$$

$$\begin{aligned}
&\boldsymbol{\theta}_3 = -\,(\boldsymbol{\varphi}_2\mathbf{B} + \mathbf{Bf}_2 + \boldsymbol{\varphi}_1\mathbf{Bf}_1)/3, \quad \boldsymbol{\gamma}_3 = (\mathbf{A}\boldsymbol{\gamma}_2 - \boldsymbol{\gamma}_2\mathbf{C} + \boldsymbol{\gamma}_1\mathbf{B}\boldsymbol{\gamma}_1)/3,\\
&\mathbf{f}_3 = (\mathbf{Af}_2 + \boldsymbol{\gamma}_2\mathbf{B} + \boldsymbol{\gamma}_1\mathbf{Bf}_1)/3, \quad \boldsymbol{\varphi}_3 = (\mathbf{B}\boldsymbol{\gamma}_2 - \boldsymbol{\varphi}_2\mathbf{C} + \boldsymbol{\varphi}_1\mathbf{B}\boldsymbol{\gamma}_1)/3,
\end{aligned} \tag{44}$$

$$\begin{aligned}
&\boldsymbol{\theta}_4 = -\,(\boldsymbol{\varphi}_3\mathbf{B} + \mathbf{Bf}_3 + \boldsymbol{\varphi}_2\mathrm{B}\boldsymbol{\varphi}_1 + \boldsymbol{\varphi}_1\mathbf{Bf}_2)/4, \quad \boldsymbol{\gamma}_4 = (\mathbf{A}\boldsymbol{\gamma}_3 - \boldsymbol{\gamma}_3\mathbf{C} + \boldsymbol{\gamma}_2\mathbf{B}\boldsymbol{\gamma}_1 + \boldsymbol{\gamma}_1\mathbf{B}\boldsymbol{\gamma}_2)/4,\\
&\mathbf{f}_4 = (\mathbf{Af}_3 + \boldsymbol{\gamma}_3\mathbf{B} + \boldsymbol{\gamma}_2\mathbf{Bf}_1 + \boldsymbol{\gamma}_1\mathbf{Bf}_2)/4, \quad \boldsymbol{\varphi}_4 = (\mathbf{B}\boldsymbol{\gamma}_3 - \boldsymbol{\varphi}_3\mathbf{C} + \boldsymbol{\varphi}_1\mathbf{B}\boldsymbol{\gamma}_2 + \boldsymbol{\varphi}_2\mathbf{B}\boldsymbol{\gamma}_1)/4.
\end{aligned} \tag{45}$$

The matrixes $\tilde{\mathbf{F}}\,(\tau)$ and $\tilde{\mathbf{E}}\,(\tau)$ are extremely small compared to the unit matrix $\mathbf{I}$ in the small interval τ. Therefore, they are calculated and stored independently to avoid losing effective digits. Here, the equations in Eqs. (41)–(45) are computationally stable since they involve only the additive and multiplicative operations except the inverse of matrices. The derivations in the former sections are exact, and the only approximation made in the precise integration method is the truncation of Taylor series expansion in Eq. (41). It will cause numerical errors; however, the errors are less than the round-off error of double-precision computation. Therefore, the method is exact in the sense that any method can be exact; i.e., it is as exact as the computer precision permits.

Once $\mathbf{F}\,(\tau)$, $\mathbf{G}\,(\tau)$, $\mathbf{Q}\,(\tau)$ and $\mathbf{E}\,(\tau)$ for a mini-layer are obtained, they are combined in the following way. Note that all mini-layers within one sub-layer have equal thickness and identical material properties; therefore, when it performs the combination of mini-layers in Eq. (38), $\mathbf{F}_1 = \mathbf{F}_2 = \mathbf{F}$, $\mathbf{G}_1 = \mathbf{G}_2 = \mathbf{G}$, $\mathbf{Q}_1 = \mathbf{Q}_2 = \mathbf{Q}$,

and $\mathbf{E}_1 = \mathbf{E}_2 = \mathbf{E}$. However, considering $\tilde{\mathbf{F}}_c$ and $\tilde{\mathbf{E}}_c$ being very small, for combination of mini-layers, Eq. (38) should be modified as

$$\begin{aligned}
&\mathbf{Q}_c = \mathbf{Q} + \left(\mathbf{I} + \tilde{\mathbf{E}}\right)\mathbf{Q}\left(\mathbf{I} + \mathbf{G}\mathbf{Q}\right)^{-1}\left(\mathbf{I} + \tilde{\mathbf{F}}\right), \quad \mathbf{G}_c = \mathbf{G} + \left(\mathbf{I} + \tilde{\mathbf{F}}\right)^{-1}\mathbf{G}\left(\mathbf{I} + \mathbf{Q}\mathbf{G}\right)^{-1}\left(\mathbf{I} + \tilde{\mathbf{E}}\right), \\
&\tilde{\mathbf{F}}_c = \left(\tilde{\mathbf{F}} - \mathbf{G}\mathbf{Q}/2\right)\left(\mathbf{I} + \mathbf{G}\mathbf{Q}\right)^{-1} + \left(\mathbf{I} + \mathbf{G}\mathbf{Q}\right)^{-1}\left(\tilde{\mathbf{F}} - \mathbf{G}\mathbf{Q}/2\right) + \tilde{\mathbf{F}}\left(\mathbf{I} + \mathbf{G}\mathbf{Q}\right)^{-1}\tilde{\mathbf{F}}, \quad \mathbf{F}_c = \mathbf{I} + \tilde{\mathbf{F}}_c, \\
&\tilde{\mathbf{E}}_c = \left(\tilde{\mathbf{E}} - \mathbf{Q}\mathbf{G}/2\right)\left(\mathbf{I} + \mathbf{Q}\mathbf{G}\right)^{-1} + \left(\mathbf{I} + \mathbf{Q}\mathbf{G}\right)^{-1}\left(\tilde{\mathbf{E}} - \mathbf{Q}\mathbf{G}/2\right) + \tilde{\mathbf{E}}\left(\mathbf{I} + \mathbf{Q}\mathbf{G}\right)^{-1}\tilde{\mathbf{E}}, \quad \mathbf{E}_c = \mathbf{I} + \tilde{\mathbf{E}}_c. \quad (46)
\end{aligned}$$

Here, in performing the mini-layer combination in Eq. (46), one should notice that the thickness of the mini-layer is extremely small. Under such condition, as stated previously, the correlation matrices $\mathbf{F}$ and $\mathbf{E}$ will tend to be unit matrices while $\mathbf{G}$ and $\mathbf{Q}$ will lead to zero. Consequently, all the formulations in Eq. (46) will remain stable.

Recursively executing Eq. (46) N_2 times, the matrices $\mathbf{F}$, $\mathbf{G}$, $\mathbf{Q}$ and $\mathbf{E}$ turn to be the correlation matrices $\mathbf{F}\left(\bar{h}_i\right)$, $\mathbf{G}\left(\bar{h}_i\right)$, $\mathbf{Q}\left(\bar{h}_i\right)$ and $\mathbf{E}\left(\bar{h}_i\right)$ of the given $\bar{h}_i$ interval (sub-layer). Such algorithm is termed as 'interval doubling.' Since matrices $\tilde{\mathbf{F}}$ and $\tilde{\mathbf{E}}$ of $\bar{h}_i$ interval are no longer very small, repeatedly employing Eq. (38) N_1 times, the correlation matrices $\mathbf{F}\left(h_i\right)$, $\mathbf{G}\left(h_i\right)$, $\mathbf{Q}\left(h_i\right)$ and $\mathbf{E}\left(h_i\right)$ of the ith layer are observed. Further combination of layers having different thickness and material properties can be directly carried out by Eq. (38).

Until now, equations of PIM to obtain the correlation matrices $\mathbf{F}$, $\mathbf{G}$, $\mathbf{Q}$ and $\mathbf{E}$ are available, and the algorithm is presented as below:

1. read the material properties and thickness h_i of the ith layer, the wavenumber k, the excitation frequency ω.
2. calculate the matrices $\mathbf{A}$, $\mathbf{B}$, $\mathbf{C}$ and $\mathbf{D}$ in Eq. (17); let $N_1 = 20$ and $N_2 = 20$, $\bar{h}_i = h_i/2^{N_1}$ and $\tau = \bar{h}_i/2^{N_2}$.
3. employ Eq. (41) to calculate $\mathbf{Q}(\tau)$, $\mathbf{G}(\tau)$, $\tilde{\mathbf{F}}(\tau)$ and $\tilde{\mathbf{E}}(\tau)$.
   $\mathbf{Q} = \mathbf{Q}(\tau)$, $\mathbf{G} = \mathbf{G}(\tau)$, $\tilde{\mathbf{F}} = \tilde{\mathbf{F}}(\tau)$ and $\tilde{\mathbf{E}} = \tilde{\mathbf{E}}(\tau)$. Comment: initiation.
4. for (iter = 0; iter $< N_2$; iter++) comment: PIM in the $\bar{h}_i$ interval.
   4.1 apply Eq. (46) to compute $\mathbf{Q}_c$, $\mathbf{G}_c$, $\tilde{\mathbf{F}}_c$ and $\tilde{\mathbf{E}}_c$;
   4.2 $\mathbf{Q} = \mathbf{Q}_c$, $\mathbf{G} = \mathbf{G}_c$, $\tilde{\mathbf{F}} = \tilde{\mathbf{F}}_c$ and $\tilde{\mathbf{E}} = \tilde{\mathbf{E}}_c$;
   end
   $\mathbf{F}\left(\bar{h}_i\right) = \mathbf{I} + \tilde{\boldsymbol{F}}_c$, $\mathbf{E}\left(\bar{h}_i\right) = \mathbf{I} + \tilde{\mathbf{E}}_c$, $\mathbf{G}\left(\bar{h}_i\right) = \mathbf{G}_c$ and $\mathbf{Q}\left(\bar{h}_i\right) = \mathbf{Q}_c$. Comment: the correlation matrices $\mathbf{F}\left(\bar{h}_i\right)$, $\mathbf{G}\left(\bar{h}_i\right)$, $\mathbf{Q}\left(\bar{h}_i\right)$ and $\mathbf{E}\left(\bar{h}_i\right)$ of the given $\bar{h}_i$ interval are obtained.
   $\mathbf{F}_1 = \mathbf{F}_2 = \mathbf{F}\left(\bar{h}_i\right)$, $\mathbf{G}_1 = \mathbf{G}_2 = \mathbf{G}\left(\bar{h}_i\right)$, $\mathbf{Q}_1 = \mathbf{Q}_2 = \mathbf{Q}\left(\bar{h}_i\right)$ and $\mathbf{E}_1 = \mathbf{E}_2 = \mathbf{E}\left(\bar{h}_i\right)$. Comment: initiation.
5. for (iter = 0; iter $< N_1$; iter++) comment: PIM in the h_i interval.
   5.1 use Eq. (38) to calculate $\mathbf{F}_c$, $\mathbf{G}_c$, $\mathbf{Q}_c$ and $\mathbf{E}_c$;
   5.2 $\mathbf{F}_1 = \mathbf{F}_2 = \mathbf{F}_c$, $\mathbf{G}_1 = \mathbf{G}_2 = \mathbf{G}_c$, $\mathbf{Q}_1 = \mathbf{Q}_2 = \mathbf{Q}_c$ and $\mathbf{E}_1 = \mathbf{E}_2 = \mathbf{E}_c$;
   end

$\mathbf{F}\left(h_i\right) = \mathbf{F}_c$, $\mathbf{G}\left(h_i\right) = \mathbf{G}_c$, $\mathbf{Q}\left(h_i\right) = \mathbf{Q}_c$ and $\mathbf{E}\left(h_i\right) = \mathbf{E}_c$. Comment: the correlation matrices $\mathbf{F}\left(h_i\right)$, $\mathbf{G}\left(h_i\right)$, $\mathbf{Q}\left(h_i\right)$ and $\mathbf{E}\left(h_i\right)$ of the ith layer are approached. Combination of layers having different thickness and material properties is directly performed by Eq. (38).

3 Green's function in the wavenumber domain

Based on the above equations, the displacements in the wavenumber domain can be obtained. As stated previously, in increasing the layer thickness, the correlation matrices $\mathbf{G}$ and $\mathbf{Q}$ will remain stable, while $\mathbf{F}$ and $\mathbf{E}$ will tend to zero; in decreasing the layer thickness, $\mathbf{F}$ and $\mathbf{E}$ will tend to be unit matrices, while $\mathbf{G}$ and $\mathbf{Q}$ will lead to zero. Considering this, to obviate the computational instability in the formulation, the following equations are given correspondingly for the two situations: (i) thin layer ($h/\lambda \ll 1$, h is the layer thickness and λ is the wavelength) and (ii) all layers except the thin layer (termed as normal layer).

To carry out the calculation, the kth layer, located with the force S (at plane $z = z_s$), should be split into two sub-layers, $k1$ and $k2$, as shown in Fig. 3. The first sub-layer $k1$ is bounded by the planes $z = z_{k-1}$ and $z = z_{s-0}$ with the thickness h_{k1}, and the second sub-layer $k2$ by $z = z_{s+0}$ and $z = z_k$ with the thickness h_{k2}. The stress in the z-direction is continuous across any interface of layers except at $z = z_s$. Considering this discontinuous, the whole layered medium is divided into two sub-domains: one is domain Γ_1 from the first

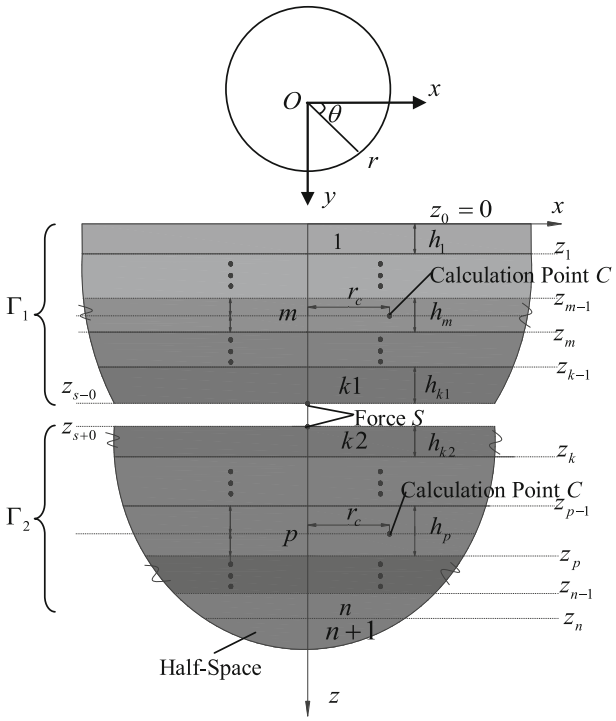

Fig. 3 Splitting the layered half-space into two domains by the force point

layer to the $k1$th layer bounded by planes $z = z_0$ and $z = z_{s-0}$, while another one corresponds to domain Γ_2 from the $k2$th layer to the nth layer bounded by planes $z = z_{s+0}$ and $z = z_n$.

In domain, Γ_1, $\bar{\mathbf{U}}_0$ and $\bar{\mathbf{P}}_0$ correspond to the displacement and stress at the free surface $z = z_0$, while $\bar{\mathbf{U}}_{k1}$ and $\bar{\mathbf{P}}_{k1}$ are the corresponding variables at the plane $z = z_{s-0}$. By recursively applying Eq. (38) in domain Γ_1, we have the following equations:

$$\bar{\mathbf{U}}_{k1} = \mathbf{F}_L\bar{\mathbf{U}}_0 - \mathbf{G}_L\bar{\mathbf{P}}_{k1}, \quad \bar{\mathbf{P}}_0 = \mathbf{Q}_L\bar{\mathbf{U}}_0 + \mathbf{E}_L\bar{\mathbf{P}}_{k1} \tag{47}$$

where the matrices $\mathbf{F}_L$, $\mathbf{G}_L$, $\mathbf{Q}_L$ and $\mathbf{E}_L$ are the correlation matrices from the first layer to the $k1$th layer.

Considering the boundary condition, the stress $\bar{\mathbf{P}}_0 = 0$ at $z = z_0$, it can obtain the stress at the plane $z = z_{s-0}$ for the case of normal layer,

$$\bar{\mathbf{P}}_{k1} = -\left(\mathbf{F}_L\mathbf{Q}_L^{-1}\mathbf{E}_L + \mathbf{G}_L\right)^{-1}\bar{\mathbf{U}}_{k1} = \mathbf{K}_1\bar{\mathbf{U}}_{k1}. \tag{48}$$

Correspondingly, for the case of a thin layer, the stress at the plane $z = z_{s-0}$ is

$$\bar{\mathbf{P}}_{k1} = -\mathbf{E}_L^{-1}\mathbf{Q}_L\left(\mathbf{F}_L + \mathbf{G}_L\mathbf{E}_L^{-1}\mathbf{Q}_L\right)^{-1}\bar{\mathbf{U}}_{k1} = \mathbf{K}_1\bar{\mathbf{U}}_{k1}. \tag{49}$$

In domain Γ_2, the combination of layers can also be carried out in an analogous approach,

$$\bar{\mathbf{U}}_n = \mathbf{F}_N\bar{\mathbf{U}}_{k2} - \mathbf{G}_N\bar{\mathbf{P}}_n, \quad \bar{\mathbf{P}}_{k2} = \mathbf{Q}_N\bar{\mathbf{U}}_{k2} + \mathbf{E}_N\bar{\mathbf{P}}_n, \tag{50}$$

where the matrices $\mathbf{F}_N$, $\mathbf{G}_N$, $\mathbf{Q}_N$ and $\mathbf{E}_N$ are the correlation matrices from the $k2$th layer to the nth layer; $\bar{\mathbf{U}}_{k2}$ and $\bar{\mathbf{P}}_{k2}$ denote the displacement and stress at the plane $z = z_{s+0}$, while $\bar{\mathbf{U}}_n$ and $\bar{\mathbf{P}}_n$ are the displacement and stress at the plane $z = z_n$.

In case of the layered medium resting on a rigid base, from Eqs. (19) and (50), it can obtain the stress at the plane $z = z_{s+0}$ for the case of a normal layer,

$$\bar{\mathbf{P}}_{k2} = \left(\mathbf{Q}_N + \mathbf{E}_N\mathbf{G}_N^{-1}\mathbf{F}_N\right)\bar{\mathbf{U}}_{k2} = \mathbf{K}_2\bar{\mathbf{U}}_{k2}. \tag{51}$$

For the case of a thin layer, one can obtain the displacement at the plane $z = z_{s+0}$,

$$\bar{\mathbf{U}}_{k2} = \mathbf{F}_N^{-1}\mathbf{G}_N \left(\mathbf{Q}_N\mathbf{F}_N^{-1}\mathbf{G}_N + \mathbf{E}_N\right)^{-1} \bar{\mathbf{P}}_{k2} = \mathbf{K}_2^{-1}\bar{\mathbf{P}}_{k2}. \tag{52}$$

Here, it should be pointed out that, when the layer is resting on a rigid base, the matrix $\mathbf{K}_2$ will become infinite, and the displacement $\bar{\mathbf{U}}_{k2}$ will tend to zero for the thin layer. It can be interpreted that, as the layer thickness decreases to that of a thin layer, the calculation point tends to be directly laid at the surface of the rigid base. As a result, the displacement will tend to zero as presented in Eq. (19), and the matrix $\mathbf{K}_2$ will become infinite.

In case the layered medium is underlaid by a semi-infinite space, substituting Eq. (25) in (50) yields the stress at the plane $z = z_{s+0}$ for both cases of normal layer and thin layer,

$$\bar{\mathbf{P}}_{k2} = \left(\mathbf{Q}_N + \mathbf{E}_N\mathbf{R}_\infty \left(\mathbf{I} + \mathbf{G}_N\mathbf{R}_\infty\right)^{-1} \mathbf{F}_N\right) \bar{\mathbf{U}}_{k2} = \mathbf{K}_2\bar{\mathbf{U}}_{k2}. \tag{53}$$

On the plane $z = z_s$, the displacements should be identical in both domains Γ_1 and Γ_2; let $\bar{\mathbf{U}}_{k1} = \bar{\mathbf{U}}_{k2} = \bar{\mathbf{U}}_s$, the total stress $\bar{\mathbf{P}}_s$ at the plane $z = z_s$ can be formulated as

$$\bar{\mathbf{P}}_s = \bar{\mathbf{P}}_{k2} - \bar{\mathbf{P}}_{k1} = \left(\mathbf{K}_2 - \mathbf{K}_1\right) \bar{\mathbf{U}}_s = \mathbf{K}\bar{\mathbf{U}}_s \tag{54}$$

which results in $\bar{\mathbf{U}}_s = \mathbf{K}^{-1}\bar{\mathbf{P}}_s$. Here, it can be observed that, when the layer thickness increases, the formulations in Eqs. (48) and (51) or (53) will remain stable since they involve only the inverse of the stable matrices $\mathbf{G}$ and $\mathbf{Q}$. In contrast, as the layer thickness decreases to that of the thin layer, the equations in Eqs. (49) and (52) or (53) should also be stable since they involve only the inverse of the stable matrices $\mathbf{F}$ and $\mathbf{E}$. Hence, the matrix $\mathbf{K}$ in Eq. (54) is indeed regular regardless of the layer thickness.

Considering Eqs. (47), (48) and (54), one can obtain the stress $\bar{\mathbf{P}}_0$ and displacement $\bar{\mathbf{U}}_0$ at the free surface $(z = z_0)$ for the case of a normal layer,

$$\bar{\mathbf{P}}_0 = 0, \quad \bar{\mathbf{U}}_0 = \mathbf{Q}_L^{-1}\mathbf{E}_L \left(\mathbf{F}_L\mathbf{Q}_L^{-1}\mathbf{E}_L + \mathbf{G}_L\right)^{-1} \mathbf{K}^{-1}\bar{\mathbf{P}}_s. \tag{55}$$

Correspondingly, the stress $\bar{\mathbf{P}}_0$ and displacement $\bar{\mathbf{U}}_0$ at the free surface $(z = z_0)$ for the case of a thin layer are

$$\bar{\mathbf{P}}_0 = 0, \quad \bar{\mathbf{U}}_0 = \left(\mathbf{F}_L + \mathbf{G}_L\mathbf{E}_L^{-1}\mathbf{Q}_L\right)^{-1} \mathbf{K}^{-1}\bar{\mathbf{P}}_s. \tag{56}$$

Analogously, the stress $\bar{\mathbf{P}}_n$ and displacement $\bar{\mathbf{U}}_n$ at the plane $z = z_n$ can be obtained from Eqs. (50), (51) or (53), and (54) for both cases of normal layer and thin layer. Here, one should consider different configurations of the bottom half-space. When the layered medium is underlaid by a semi-infinite space, one should have

$$\bar{\mathbf{P}}_n = \mathbf{R}_\infty \left(\mathbf{I} + \mathbf{G}_N\mathbf{R}_\infty\right)^{-1} \mathbf{F}_N\mathbf{K}^{-1}\bar{\mathbf{P}}_s, \quad \bar{\mathbf{U}}_n = \left(\mathbf{I} + \mathbf{G}_N\mathbf{R}_\infty\right)^{-1} \mathbf{F}_N\mathbf{K}^{-1}\bar{\mathbf{P}}_s. \tag{57}$$

When the layered medium is resting on a rigid base, one can obtain

$$\bar{\mathbf{P}}_n = \mathbf{G}_N^{-1}\mathbf{F}_N\mathbf{K}^{-1}\bar{\mathbf{P}}_s, \quad \bar{\mathbf{U}}_n = 0. \tag{58}$$

Obviously, the equations in Eqs. (55)–(58) are unconditionally stable since the inverse of the matrix only performs for the stable matrices $\mathbf{G}$ and $\mathbf{Q}$ as the layer thickness increases, or the inverse of the matrix only performs for the stable matrices $\mathbf{F}$ and $\mathbf{E}$ as the layer thickness decreases to that of a thin layer.

Until now, we obtained the stress and displacement at the free surface $z = z_0$, at the force plane $z = z_s$, and at the plane $z = z_n$. On the basis of these variables, one can easily obtain the stress and displacement at any plane $z = z_c$. Since the displacement is identical for every point at the same elevation z in the wavenumber domain [28], in the following we do not mention the displacement of which point is calculated, but only the elevation of the point.

Considering a general layer configuration model, as shown in Fig. 4, it locates a point C at the plane $z = z_c$. The corresponding stress–displacement relation can be expressed as

$$\begin{Bmatrix} \bar{\mathbf{U}}_c \\ \bar{\mathbf{P}}_t \end{Bmatrix} = \begin{bmatrix} \mathbf{F}_1 & -\mathbf{G}_1 \\ \mathbf{Q}_1 & \mathbf{E}_1 \end{bmatrix} \begin{Bmatrix} \bar{\mathbf{U}}_t \\ \bar{\mathbf{P}}_c \end{Bmatrix}, \quad \begin{Bmatrix} \bar{\mathbf{U}}_b \\ \bar{\mathbf{P}}_c \end{Bmatrix} = \begin{bmatrix} \mathbf{F}_2 & -\mathbf{G}_2 \\ \mathbf{Q}_2 & \mathbf{E}_2 \end{bmatrix} \begin{Bmatrix} \bar{\mathbf{U}}_c \\ \bar{\mathbf{P}}_b \end{Bmatrix} \tag{59}$$

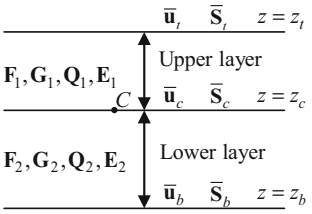

Fig. 4 Layer configuration of the analysis model

in which $\bar{\mathbf{U}}_t$ and $\bar{\mathbf{P}}_t$ are the displacement and stress at the plane $z = z_t$; $\bar{\mathbf{U}}_c$ and $\bar{\mathbf{P}}_c$ are at the plane $z = z_c$; $\bar{\mathbf{U}}_b$ and $\bar{\mathbf{P}}_b$ are at the plane $z = z_b$; $\mathbf{F}_1, \mathbf{G}_1, \mathbf{Q}_1, \mathbf{E}_1$ are the correlation matrices from the plane $z = z_t$ to the plane $z = z_c$ ($z_t \leq z_c$); $\mathbf{F}_2, \mathbf{G}_2, \mathbf{Q}_2, \mathbf{E}_2$ are the correlation matrices from the plane $z = z_c$ to the plane $z = z_b$ ($z_c \leq z_b$).

Considering the continuity condition at the plane $z = z_c$, it yields the stress $\bar{\mathbf{P}}_c$ and displacement $\bar{\mathbf{U}}_c$ for the case of a normal layer

$$\bar{\mathbf{U}}_c = \mathbf{M}\bar{\mathbf{U}}_t + \mathbf{N}\bar{\mathbf{U}}_b, \quad \bar{\mathbf{P}}_c = \mathbf{P}\bar{\mathbf{U}}_t + \mathbf{R}\bar{\mathbf{U}}_b \tag{60}$$

where $\mathbf{M} = \left(\mathbf{G}_1\mathbf{E}_2\mathbf{G}_2^{-1}\mathbf{F}_2 + \mathbf{G}_1\mathbf{Q}_2 + \mathbf{I}\right)^{-1}\mathbf{F}_1$, $\mathbf{N} = \left(\mathbf{E}_2\mathbf{G}_2^{-1}\mathbf{F}_2 + \mathbf{Q}_2 + \mathbf{G}_1^{-1}\right)^{-1}\mathbf{E}_2\mathbf{G}_2^{-1}$, $\mathbf{P} = \mathbf{G}_1^{-1}(\mathbf{F}_1 - \mathbf{M})$, $\mathbf{R} = -\mathbf{G}_1^{-1}\mathbf{N}$.

Considering that the thickness of the upper layer decreases to that of a thin layer, as stated before, the correlation matrices $\mathbf{G_1}$ and $\mathbf{Q_1}$ will tend to zero, while $\mathbf{F_1}$ and $\mathbf{E_1}$ will lead to unit matrices. Hence, the coefficient matrices in Eq. (60) should be modified to obviate the singularity problem,

$$\mathbf{M} = \boldsymbol{\Omega}\boldsymbol{F}_1, \quad \mathbf{N} = \boldsymbol{\Omega}\boldsymbol{G}_1\mathbf{E}_2\mathbf{G}_2^{-1}, \quad \mathbf{P} = \boldsymbol{\Psi}\left(\mathbf{E}_2\mathbf{G}_2^{-1}\mathbf{F}_2 + \mathbf{Q}_2\right)\mathbf{F}_1, \quad \mathbf{R} = -\boldsymbol{\Psi}\boldsymbol{E}_2\mathbf{G}_2^{-1}, \tag{61}$$

where $\boldsymbol{\Omega} = \left(\mathbf{G}_1\mathbf{E}_2\mathbf{G}_2^{-1}\mathbf{F}_2 + \mathbf{G}_1\mathbf{Q}_2 + \mathbf{I}\right)^{-1}$, $\boldsymbol{\Psi} = \left(\mathbf{E}_2\mathbf{G}_2^{-1}\mathbf{F}_2\mathbf{G}_1 + \mathbf{Q}_2\mathbf{G}_1 + \mathbf{I}\right)^{-1}$.

In case the thickness of the lower layer tends to be that of a thin layer, the correlation matrices $\mathbf{G}_2$ and $\mathbf{Q}_2$ will tend to zero, while $\mathbf{F}_2$ and $\mathbf{E}_2$ will lead to unit matrices. Thus, to eliminate the matrix singularity, the coefficient matrices in Eq. (60) should be refined as below,

$$\mathbf{M} = \boldsymbol{\Pi}\boldsymbol{G}_2\mathbf{E}_2^{-1}\mathbf{G}_1^{-1}\mathbf{F}_1, \quad \mathbf{N} = \boldsymbol{\Pi}, \quad \mathbf{P} = \mathbf{G}_1^{-1}(\mathbf{F}_1 - \mathbf{M}), \quad \mathbf{R} = -\mathbf{G}_1^{-1}\mathbf{N}, \tag{62}$$

where $\boldsymbol{\Pi} = \left(\mathbf{F}_2 + \mathbf{G}_2\mathbf{E}_2^{-1}\mathbf{Q}_2 + \mathbf{G}_2\mathbf{E}_2^{-1}\mathbf{G}_1^{-1}\right)^{-1}$.

In case both layers in Fig. 4 tend to be the thin layer, the correlation matrices $\mathbf{G}$ and $\mathbf{Q}$ for both layers will tend to zero, while $\mathbf{F}$ and $\mathbf{E}$ will lead to unit matrices. Hence, the stress $\bar{\mathbf{P}}_c$ and displacement $\bar{\mathbf{U}}_c$ at the plane $z = z_c$ are

$$\bar{\mathbf{U}}_c = \left(\bar{\mathbf{U}}_t + \bar{\mathbf{U}}_b\right)/2, \quad \bar{\mathbf{P}}_c = \left(\bar{\mathbf{P}}_t + \bar{\mathbf{P}}_b\right)/2. \tag{63}$$

Apparently, Eqs. (60)–(63) are computationally stable formulations since the inverse of the matrix only performs for the stable matrices $\mathbf{G}$ and $\mathbf{Q}$ as the layer thickness increases, or the inverse only performs for the stable matrices $\mathbf{F}$ and $\mathbf{E}$ as the layer thickness decreases to that of a thin layer. Equations (60)–(63) are the general formulations for the derivation of the stress and displacement at the point C ($z = z_c$). To be specific, there are three different conditions existing due to the position of point C (Fig. 3): above the force, below the force and on the plane of the force. For the last case, since the displacement is identical for points at the same elevation z in the wavenumber domain [28], the stress–displacement relation can be directly obtained via Eq. (54). Hence, we only need to consider the first two conditions. In case the calculation point C is above the force (in the mth layer, as shown in Fig. 3), one should consider $\bar{\mathbf{U}}_t = \bar{\mathbf{U}}_0$ and $\bar{\mathbf{U}}_b = \bar{\mathbf{U}}_s$ in Eqs. (60)–(63) to obtain the stress and displacement at the point C. Here, $\bar{\mathbf{U}}_0$ and $\bar{\mathbf{U}}_s$ are obtained from Eqs. (54) and (55) or (56), respectively. In case the calculation point C is below the force (in the pth layer, as shown in Fig. 3), one should consider $\bar{\mathbf{U}}_t = \bar{\mathbf{U}}_s$ and $\bar{\mathbf{U}}_b = \bar{\mathbf{U}}_n$ in Eqs. (60)–(63) to obtain the stress and displacement at the point C. Here, $\bar{\mathbf{U}}_s$ and $\bar{\mathbf{U}}_n$ are obtained from Eqs. (54) and (57) or (58), respectively.

It is worthwhile to note that, if the layer thickness is zero, the correlation matrices should be set as

$$\mathbf{F} = \mathbf{E} = \mathbf{I}, \quad \mathbf{G} = \mathbf{Q} = 0. \tag{64}$$

Generally, the above formulations to calculate the stress and displacement at point C are unconditionally stable. From Eq. (60), the displacement at point C can be written in a matrix form,

$$\bar{\mathbf{U}}_c = \bar{\mathbf{G}}(k)\,\bar{\mathbf{P}}_s = \begin{bmatrix} \bar{G}_{rr}(k,z_c) & 0 & \bar{G}_{zr}(k,z_c) \\ 0 & \bar{G}_{\theta\theta}(k,z_c) & 0 \\ \bar{G}_{rz}(k,z_c) & 0 & \bar{G}_{zz}(k,z_c) \end{bmatrix} \begin{Bmatrix} \bar{\tau}_{rz}(k,z_s) \\ \bar{\tau}_{\theta z}(k,z_s) \\ \bar{\sigma}_{zz}(k,z_s) \end{Bmatrix}, \tag{65}$$

where $\bar{\mathbf{U}}_c = \{\bar{u}_r, \bar{u}_\theta, \bar{u}_z\}^{\mathrm{T}}$ denotes the displacement at point C; $\bar{\mathbf{G}}(k)$ represents the flexibility matrix (displacement Green's function in the wavenumber domain), which is a function of z, k and ω only. $\bar{\tau}_{rz}(k,z_s)$, $\bar{\tau}_{\theta z}(k,z_s)$ and $\bar{\sigma}_{zz}(k,z_s)$ are the radial, circumferential and vertical stress of force S in the wavenumber domain, which can be calculated similarly by Eq. (8) via substituting the displacement vector with the stress vector.

Similarly, from Eq. (60), the stress vector at point C can also be formulated in a matrix form,

$$\bar{\mathbf{P}}_c = \bar{\mathbf{S}}(k)\,\bar{\mathbf{P}}_s = \begin{bmatrix} \bar{S}_{rr}(k,z_c) & 0 & \bar{S}_{zr}(k,z_c) \\ 0 & \bar{S}_{\theta\theta}(k,z_c) & 0 \\ \bar{S}_{rz}(k,z_c) & 0 & \bar{S}_{zz}(k,z_c) \end{bmatrix} \begin{Bmatrix} \bar{\tau}_{rz}(k,z_s) \\ \bar{\tau}_{\theta z}(k,z_s) \\ \bar{\sigma}_{zz}(k,z_s) \end{Bmatrix}, \tag{66}$$

where $\bar{\mathbf{P}}_c = \{\bar{\tau}_{rz}, \bar{\tau}_{\theta z}, \bar{\sigma}_{zz}\}^{\mathrm{T}}$ denotes the stress vector at point C; $\bar{\mathbf{S}}(k)$ is the relation matrix between the force S and the stress at point C, which is a function of z, k and ω only.

From Eqs. (16), (65) and (66), one can obtain the derivation of displacement and stress with respect to z in the wavenumber domain,

$$\frac{\mathrm{d}\bar{\mathbf{U}}_c}{\mathrm{d}z} = \mathbf{A}\bar{\mathbf{U}}_c + \mathbf{D}\bar{\mathbf{P}}_c, \quad \frac{\mathrm{d}\bar{\mathbf{P}}_c}{\mathrm{d}z} = \mathbf{B}\bar{\mathbf{U}}_c + \mathbf{C}\bar{\mathbf{P}}_c, \tag{67}$$

where the coefficient matrices $\mathbf{A}$, $\mathbf{B}$, $\mathbf{C}$ and $\mathbf{D}$ can be obtained from Eq. (17).

In order to verify the proposed approach, calculations are performed for the homogeneous transversely isotropic semi-infinite space. When a unit point load locates on the free surface, there are analytical solutions for the surface displacement Green's function in the wavenumber domain [11]. Comparisons are made with the results obtained from the proposed method and analytical solutions. The homogeneous transversely isotropic semi-infinite space with normalized parameters is investigated here. The material properties are: material density $\bar{\rho} = 1$, Young's moduli $\bar{E} = 2.6$ and $\bar{E}' = 2.0$, Poisson's ratios $\nu = 0.3$ and $\nu' = 1/3$, shear modulus $\bar{G}' = 1.0$, material damping ratios $\xi = \xi' = 0.05$. For highlighting the advantages of the proposed method, the homogenous semi-infinite space is artificially split into three sub-layers plus a semi-infinite space. Thus, it approaches a multi-layered medium but with identical material properties. The thickness of each sub-layer is flexible, which has no influence on the results. Here, the thicknesses of the three sub-layers are set as $h_1 = h, h_2 = 0.00001h$ and $h_3 = 3h$, which comprises both normal layer thickness and thin ones. The normalized excitation frequency is $a_0 h = \omega h\sqrt{\rho_0/d_{66}^0} = 5$.

The horizontal component $\bar{G}_{rr}(k, z=0)$ and vertical component $\bar{G}_{zz}(k, z=0)$ of displacement Green's function are presented in Fig. 5. In the figure, the real and imaginary parts of the solutions are depicted. It

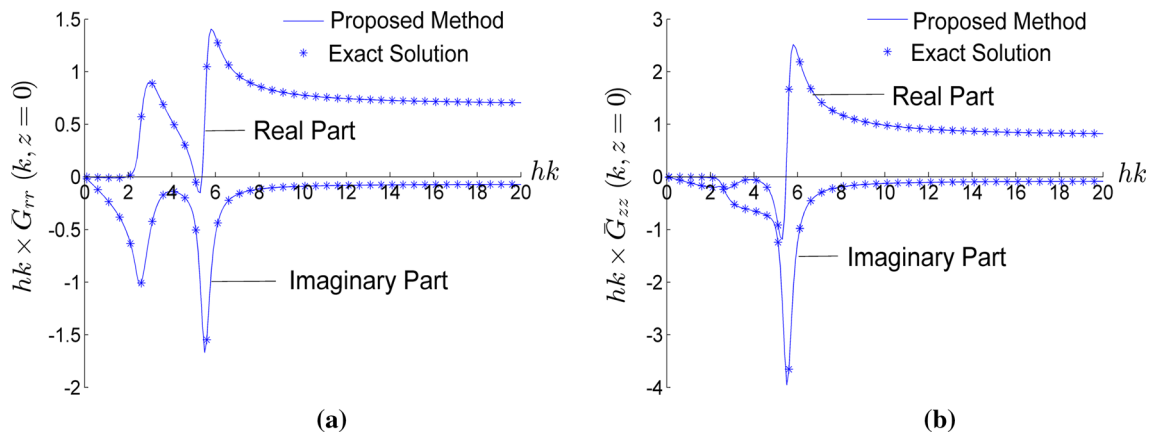

Fig. 5 Displacement Green's function in the wavenumber domain. Here, the homogeneous semi-infinite space is considered. **a** Horizontal component, **b** vertical component

can be observed that both results coincide, which indicates that excellent agreements between the proposed method and the analytical solutions are achieved.

4 Green's function in the spatial domain

From Eqs. (8) and (65), the displacement in the spatial domain can be obtained,

$$\mathbf{U}(r,\theta,z)=\sum_{n=0}^{\infty}\mathbf{T}(n\theta)\int_{k=0}^{\infty}k\mathbf{C}_n(kr)\,\bar{\mathbf{U}}(k,z,n)\mathrm{d}k=\sum_{n=0}^{\infty}\mathbf{T}(n\theta)\int_{k=0}^{\infty}k\mathbf{C}_n(kr)\,\bar{\mathbf{G}}(k)\,\bar{\mathbf{P}}_s(k)\mathrm{d}k, \tag{68}$$

where $\mathbf{U}(r,\theta,z)=(u_r,u_\theta,u_z)^{\mathrm{T}}$; $\bar{\mathbf{P}}_s(k)$ being the transform of the loads in the wavenumber domain, which can be calculated similarly by Eq. (8) via substituting the displacement vector with the stress vector.

Here, the derivation of the displacement with respect to r, θ and z can be obtained from Eq. (68):

$$\begin{aligned}
\frac{\mathrm{d}\mathbf{U}(r,\theta,z)}{\mathrm{d}r}&=\sum_{n=0}^{\infty}\mathbf{T}(n\theta)\int_{k=0}^{\infty}k\frac{\mathrm{d}\mathbf{C}_n(kr)}{\mathrm{d}r}\bar{\mathbf{G}}(k)\,\bar{\mathbf{P}}_s(k)\mathrm{d}k,\\
\frac{\mathrm{d}\mathbf{U}(r,\theta,z)}{\mathrm{d}\theta}&=\sum_{n=0}^{\infty}\frac{\mathrm{d}\mathbf{T}(n\theta)}{\mathrm{d}\theta}\int_{k=0}^{\infty}k\mathbf{C}_n(kr)\,\bar{\mathbf{G}}(k)\,\bar{\mathbf{P}}_s(k)\mathrm{d}k,\\
\frac{\mathrm{d}\mathbf{U}(r,\theta,z)}{\mathrm{d}z}&=\sum_{n=0}^{\infty}\mathbf{T}(n\theta)\int_{k=0}^{\infty}k\mathbf{C}_n(kr)\frac{\mathrm{d}\bar{\mathbf{U}}(k,z,n)}{\mathrm{d}z}\mathrm{d}k
\end{aligned} \tag{69}$$

in which

$$\frac{\mathrm{d}\mathbf{C}_n(kr)}{\mathrm{d}r}=\begin{bmatrix}
k\frac{\mathrm{d}^2J_n(kr)}{\mathrm{d}(kr)^2} & nk\left(\frac{1}{kr}\frac{\mathrm{d}J_n(kr)}{\mathrm{d}(kr)}-\frac{J_n(kr)}{(kr)^2}\right) & 0\\
nk\left(\frac{1}{kr}\frac{\mathrm{d}J_n(kr)}{\mathrm{d}(kr)}-\frac{J_n(kr)}{(kr)^2}\right) & k\frac{\mathrm{d}^2J_n(kr)}{\mathrm{d}(kr)^2} & 0\\
0 & 0 & -k\frac{\mathrm{d}J_n(kr)}{\mathrm{d}(kr)}
\end{bmatrix}. \tag{70}$$

The diagonal matrix $\mathbf{T}(n\theta)$ is $\frac{\mathrm{d}\mathbf{T}(n\theta)}{\mathrm{d}\theta}=-n\mathrm{diag}[\sin n\theta,\cos n\theta,\sin n\theta]$ for the symmetric case about the x axis (the r axis at $\theta=0$), and $\frac{\mathrm{d}\mathbf{T}(n\theta)}{\mathrm{d}\theta}=n\mathrm{diag}[\cos n\theta,-\sin n\theta,\cos n\theta]$ for the anti-symmetric case. θ is the angle of revolution around the x axis.

From Eqs. (65)–(67) and (69), the derivation of the displacement with respect to z can be obtained,

$$\frac{\mathrm{d}\mathbf{U}(r,\theta,z)}{\mathrm{d}z}=\sum_{n=0}^{\infty}\mathbf{T}(n\theta)\int_{k=0}^{\infty}k\mathbf{C}_n(kr)\left[\mathbf{A}\bar{\mathbf{G}}(k)+\mathbf{D}\bar{\mathbf{S}}(k)\right]\bar{\mathbf{P}}_s\mathrm{d}k. \tag{71}$$

Substituting Eqs. (69) and (71) in Eq. (6), one can obtain the strain $\boldsymbol{\varepsilon}=\left[\varepsilon_{rr},\varepsilon_{\theta\theta},\varepsilon_{zz},\varepsilon_{\theta z},\varepsilon_{rz},\varepsilon_{r\theta}\right]^{\mathrm{T}}$ in the spatial domain. Then, substituting the strain $\boldsymbol{\varepsilon}$ in Eq. (1), the stress $\boldsymbol{\sigma}$ in the spatial domain is obtained, which can be expressed in a matrix form,

$$\boldsymbol{\sigma}(r,\theta,z)=\begin{bmatrix}\sigma_{rr}\\ \sigma_{\theta\theta}\\ \sigma_{zz}\\ \tau_{\theta z}\\ \tau_{rz}\\ \tau_{r\theta}\end{bmatrix}=\mathbf{S}\Gamma=\begin{bmatrix}
S_{xrr} & S_{yrr} & S_{zrr}\\
S_{x\theta\theta} & S_{y\theta\theta} & S_{z\theta\theta}\\
S_{xzz} & S_{yzz} & S_{zzz}\\
S_{x\theta z} & S_{y\theta z} & S_{z\theta z}\\
S_{xrz} & S_{yrz} & S_{zrz}\\
S_{xr\theta} & S_{yr\theta} & S_{zr\theta}
\end{bmatrix}\begin{Bmatrix}\Gamma_x(r_s,\theta_s,z_s)\\ \Gamma_y(r_s,\theta_s,z_s)\\ \Gamma_z(r_s,\theta_s,z_s)\end{Bmatrix}, \tag{72}$$

where $\boldsymbol{\Gamma}$ represents the resultant force of the applied load; (r_s,θ_s,z_s) denotes the coordinate of the force S; $\mathbf{S}$ is the stress Green's function matrix in the spatial domain; elements S_{ijl} $(i=x,y,z;\ j=r,\theta,z;\ l=r,\theta,z)$ represent the stress in the j direction at point (r,θ,z) when a unit load is applied in the i direction at point (r_s,θ_s,z_s); here, l is the direction of the normal of the infinitesimal area that the stress component acts on.

Thus, we complete the formulation and can proceed to the calculation of the Green's function in the spatial domain for various load conditions. In the following, we will present an example for the evaluation of the

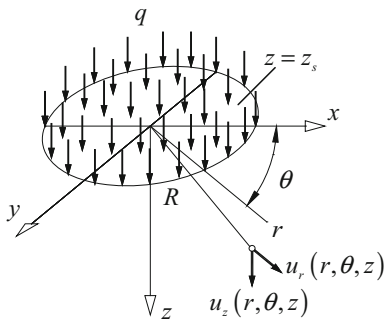

Fig. 6 Displacement under the uniformly distributed load on a disk

displacement Green's function in detail for better illustration. The Green's function for other load conditions could be calculated similarly as in the example.

It assumes an uniformly distributed vertical load of amplitude q acting on a sub-disk of radius R at the plane $z = z_s$, as shown in Fig. 6. This case corresponds to the zeroth symmetric case ($n = 0$) in Eq. (8). Formulating the equation leads to the load in the wavenumber domain,

$$\bar{\sigma}_{zz}(k) = \frac{1}{2\pi}\int_{r=0}^{R} r J_0(kr)\int_{\theta=0}^{2\pi} q\,\mathrm{d}\theta\mathrm{d}r = \frac{qR}{k}J_1(kR). \tag{73}$$

Substituting Eq. (73) in (68), one can obtain the displacement in the spatial domain,

$$\begin{Bmatrix} u_r(r,\theta,z) \\ u_\theta(r,\theta,z) \\ u_z(r,\theta,z) \end{Bmatrix} = qR\int_{k=0}^{\infty} J_1(kR)\begin{Bmatrix} \bar{G}_{zr}(k)\,J_1(kr) \\ 0 \\ \bar{G}_{zz}(k)\,J_0(kr) \end{Bmatrix}\mathrm{d}k. \tag{74}$$

The displacement for the vertical ring load can be obtained from the previous results for a disk load by simple algebraic manipulations. If $\hat{\boldsymbol{U}}(r,\zeta)$ represents the displacement due to a ring load q with radius ζ, and $\mathbf{U}(r,R)$ denotes the displacement due to a disk load having radius R with intensity $q(R) = q$, then

$$\mathbf{U}(r,R) = \int_{\zeta=0}^{R}\hat{\boldsymbol{U}}(r,\zeta)\,\mathrm{d}\zeta, \quad \hat{\boldsymbol{U}}(r,R) = \frac{\partial\mathbf{U}(r,R)}{\partial R}. \tag{75}$$

Therefore, the displacement due to the vertical ring load is obtained by employing derivation with respect to R in Eq. (74). The final equations are

$$\begin{Bmatrix} u_r(r,\theta,z) \\ u_\theta(r,\theta,z) \\ u_z(r,\theta,z) \end{Bmatrix} = qR\int_{k=0}^{\infty} kJ_0(kR)\begin{Bmatrix} \bar{G}_{zr}(k)\,J_1(kr) \\ 0 \\ \bar{G}_{zz}(k)\,J_0(kr) \end{Bmatrix}\mathrm{d}k. \tag{76}$$

The displacement for a vertical point load can be obtained from those for a disk load by considering the limit when R tends to zero. In the case of a load with intensity Q, the corresponding stress is $q = Q/\pi R^2$. The limit expression for the displacement due to a vertical point load when $R \to 0$ is

$$\begin{Bmatrix} u_r(r,\theta,z) \\ u_\theta(r,\theta,z) \\ u_z(r,\theta,z) \end{Bmatrix} = \frac{Q}{\pi}\int_{k=0}^{\infty} k\begin{Bmatrix} \bar{G}_{zr}(k)\,J_1(kr) \\ 0 \\ \bar{G}_{zz}(k)\,J_0(kr) \end{Bmatrix}\mathrm{d}k. \tag{77}$$

The force–displacement relation, obtained by Eqs. (68), (74), (76) and (77) in the cylindrical coordinate system, can be expressed in matrix form as

$$\begin{Bmatrix} u_r(r,\theta,z) \\ u_\theta(r,\theta,z) \\ u_z(r,\theta,z) \end{Bmatrix} = \mathbf{G}\Gamma = \begin{bmatrix} G_{xr} & G_{yr} & G_{zr} \\ G_{x\theta} & G_{y\theta} & G_{z\theta} \\ G_{xz} & G_{yz} & G_{zz} \end{bmatrix}\begin{Bmatrix} \Gamma_x(r_s,\theta_s,z_s) \\ \Gamma_y(r_s,\theta_s,z_s) \\ \Gamma_z(r_s,\theta_s,z_s) \end{Bmatrix} \tag{78}$$

where $\mathbf{\Gamma}$ represents the resultant force of the applied load, $\Gamma = \pi R^2 q$ (uniformly distributed load), $\Gamma = 2\pi Rq$ (ring load) and $\Gamma = Q$ (point load); (r_s, θ_s, z_s) denotes the coordinate of the force S; $\mathbf{G}$ is the displacement Green's function matrix in the spatial domain; elements G_{ij}, $(i = x, y, z;\ j = r, \theta, z)$ represent the flexibility coefficient, which indicates the displacement in the j direction at point (r, θ, z) when a unit load is applied in the i direction at point (r_s, θ_s, z_s).

5 Approach of numerical integration

The infinite integrals of Green's function in Eqs. (68), (69) and (72) can be integrated numerically. It is worthwhile to note that the integrands involve Bessel functions, which are oscillation functions and tend to zero slowly with the rise of the variable. A common numerical integration method, such as Simpson's rule or trapezoidal rule, is inadequate to achieve sufficient accuracy [49]. The method employed in this work is the adaptive Gauss quadrature from Chave [43] and Lucas [44]. Due to the difference of the integrands in the distributed, ring and point load cases, the integrations should be performed separately.

For the evaluation of Green's function under the point load, such as Eq. (77), the integrands involve only one Bessel function $J_m(kr)$. The integration can be easily performed by the method of Chave [43]. The detailed theoretical derivation of the method can be found in [43]. Here, only the concept of the method will be briefly introduced. To perform the integrations involving one Bessel function, the integrals are expressed as a finite sum of a sequence of partial integral terms,

$$I = \int_0^\infty f(k, z)\, J_m(kr)\, \mathrm{d}k \approx \sum_{n=1}^{N} I_n = \sum_{n=1}^{N} \int_{k_n}^{k_{n+1}} f(k, z)\, J_m(kr)\, \mathrm{d}k \tag{79}$$

where k_n is the nth zero of $J_m(x)$ normalized by the range r.

Every partial integral terms I_n are evaluated by the Gauss–Legendre quadrature. A combined relative–absolute error criterion is employed to terminate the calculation. If the error criterion is not satisfied, new Gauss points are added. At each step, it retains the integral kernel and Bessel function values so that only the new integrand values need to be calculated. The complete integral is formally obtained by summing the partial integrals. Due to the Bessel function's oscillatory behavior, the convergence of the result will be very slow, and the divergence maybe happen if the integral kernel increases faster than $k^{1/2}$. In [43], the continued fraction approach is used for the summation of the integral. We therefore adopt this algorithm. In the following examples, the relative and absolute errors are set as 10^{-6} and 10^{-7}. A three-point Gauss rule is firstly employed with extension to 7, 15, 31, 63, 127 and 255 common-point interlacing forms, which corresponds to integrating polynomials of degree 5, 11, 23, 47, 95, 191 and 383, respectively.

For the evaluation of Green's function under distributed load or ring load, such as Eqs. (74) and (76), there are products of Bessel functions of different orders, $J_m(kR)\, J_n(kr)$. It cannot be directly integrated by the method of Chave. It has been studied by Lucas [44] employing adaptive Gauss quadrature. The details of the method can be found in [44]. Here, we will briefly introduce the concept behind the method.

The infinite integral of products of Bessel functions is expressed as a summation of two integrals

$$I = \int_0^\infty f(k, z)\, J_m(kR)\, J_n(kr)\, \mathrm{d}k = \int_0^{k_{\max}} f(k, z)\, J_m(kR)\, J_n(kr)\, \mathrm{d}k + \int_{k_{\max}}^\infty f(k, z)\, J_m(kR)\, J_n(kr)\, \mathrm{d}k \tag{80}$$

where $k_{\max}$ is the largest of the first zeros of $Y_m(kR)$ and $Y_n(kr)$; $Y_m(kR)$ and $Y_n(kr)$ are the Bessel functions of the second kind. Both the finite and infinite integrals at the right-hand side in Eq. (80) are then evaluated by the adaptive Gauss quadrature of Chave [43]. To facilitate the calculation, ε-algorithm and mW transform are used to achieve high accuracy and efficiency.

6 Examples: horizontal and vertical point loads

To validate the present solutions, four types of soil medium are considered: homogenous transversely isotropic semi-infinite space, isotropic five-layered semi-infinite space, transversely isotropic four-layered semi-infinite space and transversely isotropic five-layered semi-infinite space. The first three cases are employed to validate the theory by comparing with the solutions available in the literature, while the last one is presented to illustrate the capability of the proposed method for the analysis of a transversely isotropic arbitrarily layered medium.

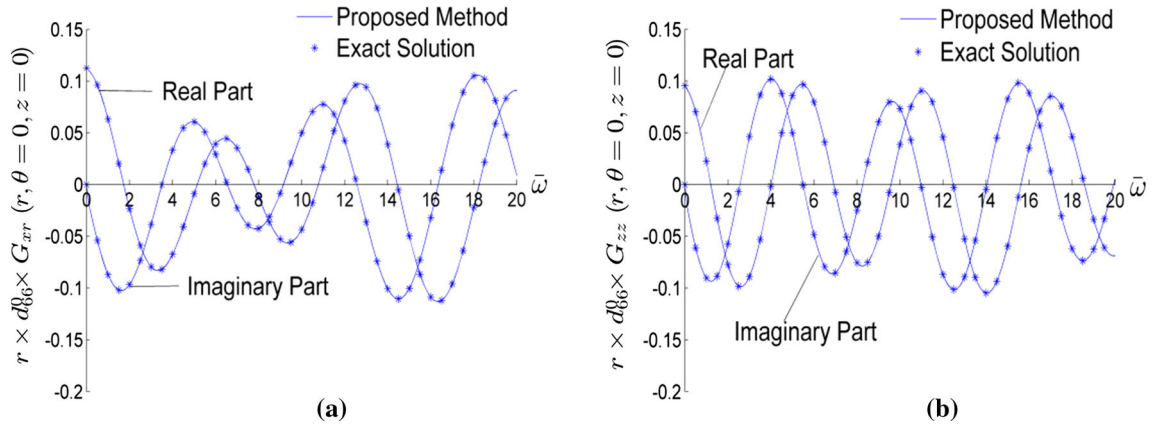

Fig. 7 Displacement Green's function in the spatial domain. Here, the homogenous semi-infinite space is considered. The point load is applied at its free surface. **a** Horizontal component, **b** vertical component

6.1 Comparison with the exact solution

Considering the case of a homogeneous transversely isotropic semi-infinite space, it is loaded with a unit harmonic point load at its free surface. The normalized material properties of the medium are: material density $\bar{\rho} = 1$, Young's moduli $\bar{E} = 2.5$ and $\bar{E}' = 4.0$, Poisson's ratios $\nu = 0.25$ and $\nu' = 0.4$, shear modulus $\bar{G}' = 2.0$, material damping ratios $\xi = 0.03$ and $\xi' = 0.05$. The displacement (Green's function) under the point load can be obtained from Eq. (78). Also, an exact solution for this case can be obtained from the work of Seale et al. [11]. Here the exact solution formulates the functions with the continuum theory in the wavenumber domain and integrates numerically by the adaptive Gauss quadrature proposed by Chave [43]; see Eq. (79). Comparisons are made between the proposed approach and the exact solution. Two cases are considered within the comparisons: the horizontal component of displacement Green's function $G_{xr}\ (r, \theta = 0, z = 0)$ and vertical component $G_{zz}\ (r, \theta = 0, z = 0)$. In the calculation, for highlighting the advantages of the proposed method, it artificially splits the homogenous semi-infinite space into four sub-layers plus a semi-infinite space. Thus, it approaches a multi-layered medium but with identical material properties. Without loss of generality, the thicknesses of the four sub-layers are set as $h_1 = 5r, h_2 = 2r, h_3 = 0.0005r$ and $h_4 = r$. It comprises both normal layer thickness and thin ones. Here, r is the radius of the calculation point. Figure 7 shows the results of the comparison. The real and imaginary parts of the results are presented. $\bar{\omega}$ denotes the normalized frequency, $\bar{\omega} = a_0 r = \omega r \sqrt{\rho_0 / d_{66}^0}$ [Eq. (4)]. It can be observed that both results coincide, which indicates that the proposed approach leads to the correct results.

6.2 Comparison with the thin-layer method

In order to validate the proposed procedure suitable for the analysis of a layered medium, comparison with the thin-layer method (TLM) [45] is performed. The isotropic five-layered semi-infinite space, subject to a unit vertical harmonic point load, is considered here, as shown in Fig. 8a. The point load is applied at $(0, 0, h)$. In the case of an isotropic medium, the following relations between the material constants are valid:

$$d_{11} = d_{33} = \lambda + 2\mu, \quad d_{13} = \lambda, \quad d_{44} = d_{66} = \mu, \quad \xi = \xi' \tag{81}$$

where λ and μ are Lamé constants. The corresponding values for the soil medium are shown in Fig. 8a. In the analysis, the thickness is set as $r/h = 1$ (r radius of the calculation point), and the damping ratio is assumed as $\xi = 0.05$.

For the implementation of the thin-layer method, the thickness of the thin layers is determined as: There are 8 thin layers inside 1 shear wavelength, $2\pi c_s / \omega d = 8$ [45]. Here, d is the thickness of the thin layer, and c_s is the shear wave velocity of the corresponding layer. Moreover, the interpolation for displacement within thin layers is cubic interpolation. To consider the radiation condition in the semi-infinite space, the space is

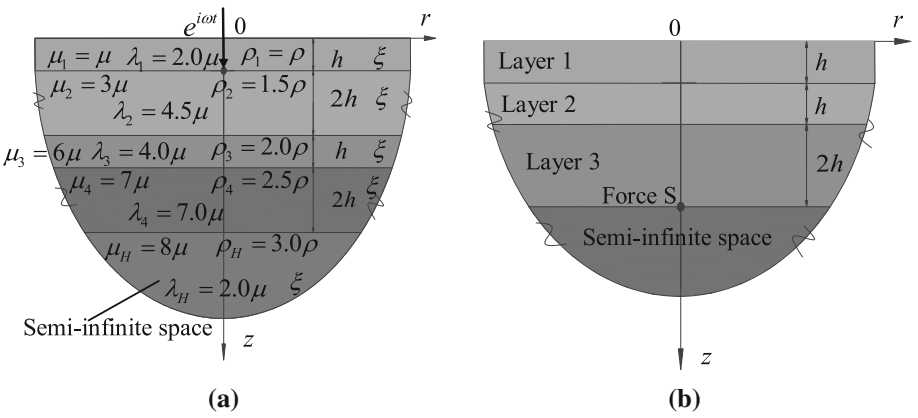

Fig. 8 Multi-layered semi-infinite space with point load. **a** Isotropic medium, **b** transversely isotropic medium

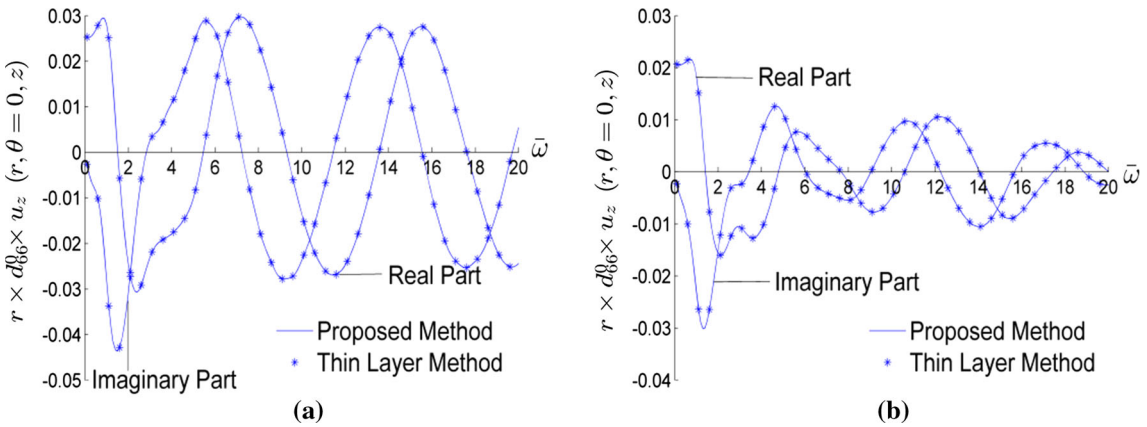

Fig. 9 Vertical displacement in the spatial domain. **a** On the plane $z = h$, **b** on the plane $z = 2h$

idealized as a thick buffer layer and a paraxial boundary with second-order approximation [11,50]. To ensure high accuracy, the thickness of the buffer layer is set as $D = 500r$ [50].

Two examples are illustrated here, differing in the depth of the calculation point: on the plane $z = h$ and $z = 2h$. The results are shown in Fig. 9. The vertical component of displacement $u_z\,(r, \theta = 0, z)$ is plotted versus the normalized frequency $\bar{\omega} = a_0 r = \omega r\sqrt{\rho_0/d_{66}^0}$ $(d_{66}^0 = \mu)$. Both the real and imaginary parts are presented. It can be observed that almost identical results are produced for the real part as well as for the imaginary part.

6.3 Comparison for a transversely isotropic multi-layered medium

To illustrate the accuracy of the proposed method for the analysis of a transversely isotropic multi-layered medium, the numerical solutions presented by Khojasteh et al. [25] for the displacement u_z and stress σ_{zz} due to a unit vertical point load are used in the comparison. The configuration of the transversely isotropic four-layered semi-infinite space is shown in Fig. 8b. The point load is applied at $(0, \theta, 4h)$. The normalized material properties are considered here and presented in Table 1. The comparison is shown in Fig. 10. The vertical displacement $u_z\,(0, \theta, z)$ and stress $\sigma_{zz}\,(0, \theta, z)$ are plotted versus the normalized depth z/h. Here, the results of $a_0 h = \omega h\sqrt{\rho_0/d_{66}^0} = 2$ are concerned. As indicated in Fig. 10, excellent agreement between the two solutions is achieved. Also, it is worthwhile to note that the imaginary part of the solutions is continuous across the loaded plane, while the real part is singular at the loaded plane. This is consistent with the analysis of Khojasteh et al. [25].

Table 1 Properties of the transversely isotropic four-layered medium

	Engineering constants						Elastic constants				
	$\bar{\rho}$	$\bar{E}$	$\bar{E}'$	$\bar{G}'$	ν	ν'	$\bar{d}_{11}$	$\bar{d}_{13}$	$\bar{d}_{33}$	$\bar{d}_{44}$	$\bar{d}_{66}$
Layer 1	1.0	2.5	3.0	1.0	0.25	0.25	2.94	0.97	3.48	1.0	1.0
Layer 2	1.1	3.0	4.0	1.4	0.25	0.25	3.49	1.14	4.57	1.4	1.2
Layer 3	1.3	5.0	5.0	2.0	0.25	0.25	6.00	2.0	6.00	2.0	2
Semi-infinite space	1.5	7.5	6.0	2.5	0.25	0.25	9.32	3.16	7.58	2.5	3

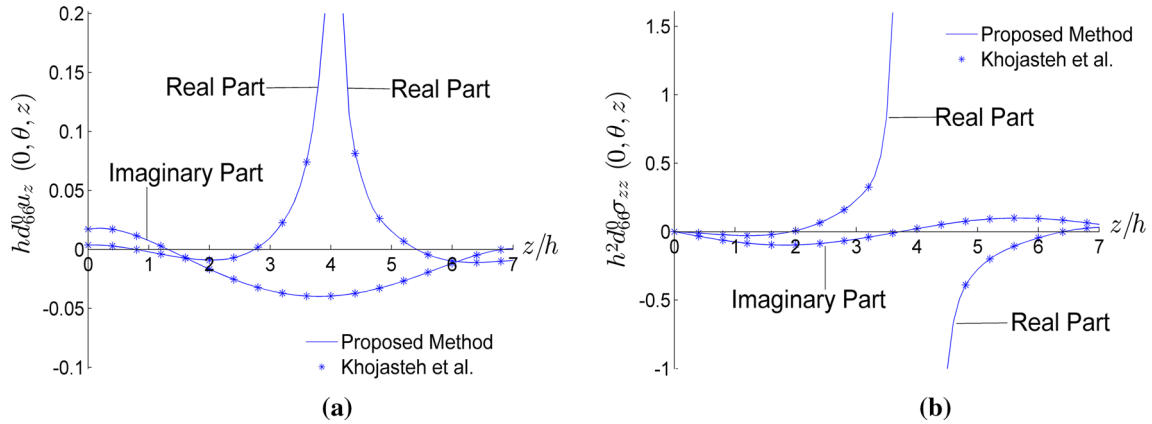

Fig. 10 Comparison of the Green's function for the transversely isotropic four-layered semi-infinite space. **a** Displacement Green's function, **b** stress Green's function

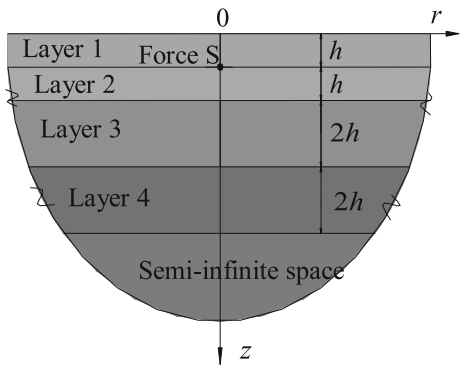

Fig. 11 Five-layered semi-infinite space with point load

Table 2 Properties of the transversely isotropic five-layered medium

	Engineering constants						Damping ratio		Elastic constants				
	$\bar{\rho}$	$\bar{E}$	$\bar{E}'$	$\bar{G}'$	ν	ν'	ξ	ξ'	$\bar{d}_{11}$	$\bar{d}_{13}$	$\bar{d}_{33}$	$\bar{d}_{44}$	$\bar{d}_{66}$
Layer 1	1.0	2.4	2.5	2.0	0.2	0.25	0.03	0.03	2.77	0.88	2.94	2.0	1.0
Layer 2	1.1	2.6	5.2	1.5	0.4	0.3	0.05	0.05	3.48	1.53	6.12	1.5	0.93
Layer 3	1.3	4.0	4.0	3.5	0.2	0.1	0.04	0.04	4.23	0.51	4.1	3.5	5/3
Layer 4	1.5	5.0	6.0	2.5	1/3	0.4	0.03	0.03	8.13	5.0	10.0	2.5	1.88
Semi-infinite space	1.7	7.5	6.0	3.0	0.3	0.4	0.06	0.06	15.4	10.0	14.0	3.0	2.88

6.4 Green's function for a transversely isotropic layered semi-infinite space

To illustrate the capability of the proposed method for the analysis of a transversely isotropic arbitrarily layered medium, a five-layered semi-infinite space shown in Fig. 11 is employed. It is subject to a unit harmonic point load at point $(0, 0, h)$. In the analysis, the thickness is set as $r/h = 1$ (r radius of the calculation point). The normalized material properties are considered here and presented in Table 2.

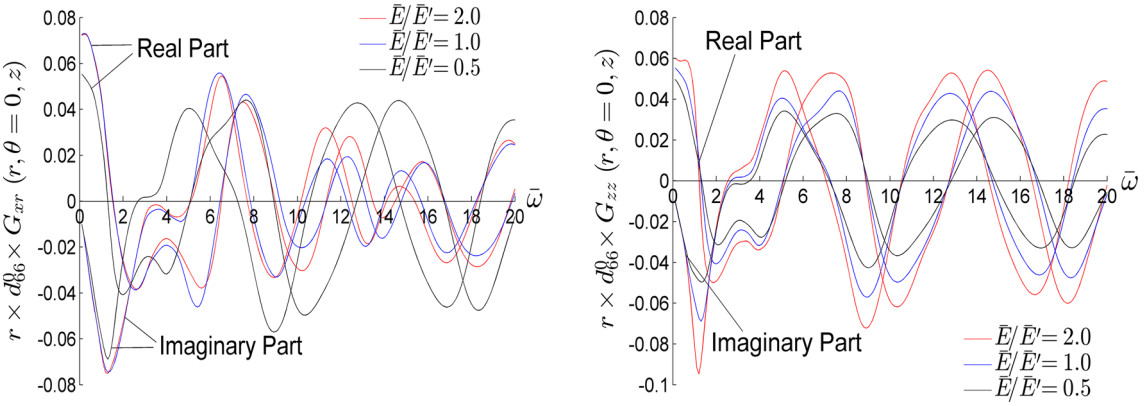

Fig. 12 Effect of soil anisotropy ($\bar{E}/\bar{E}'$) on the displacement ($z = h$)

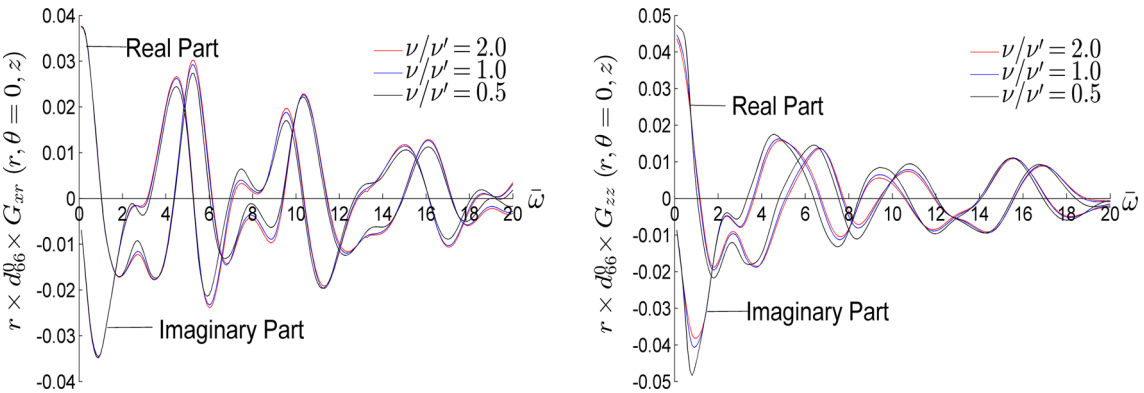

Fig. 13 Effect of soil anisotropy (ν/ν') on the displacement ($z = 2h$)

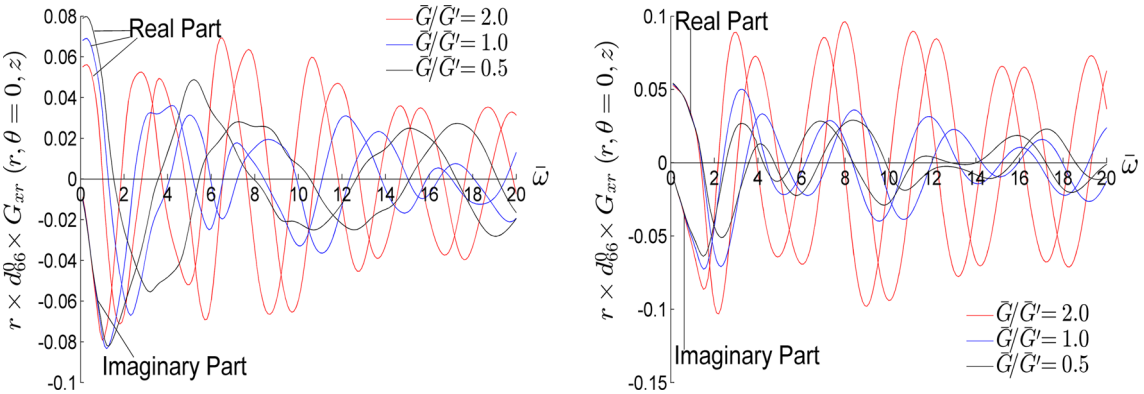

Fig. 14 Effect of soil anisotropy ($\bar{G}/\bar{G}'$) on the displacement ($z = 0$)

Also, it investigates the effect of the degree of anisotropy on the displacement. The degree of anisotropy includes the ratios $\bar{E}/\bar{E}'$, ν/ν' and $\bar{G}/\bar{G}'$ (i.e., $\bar{G} = \bar{d}_{66}$). Here, the change in the degree of anisotropy implements at the close layer below the calculation point. For instance, when the calculation point is at the plane $z = h$, we will only modify the ratios $\bar{E}/\bar{E}'$, ν/ν' and $\bar{G}/\bar{G}'$ for Layer 2. Moreover, we will fix $\bar{E}$, ν and $\bar{G}$ and change $\bar{E}'$, ν' and $\bar{G}'$ to achieve the corresponding ratios $\bar{E}/\bar{E}'$, ν/ν' and $\bar{G}/\bar{G}'$. Illustrative examples consist of the horizontal component of displacement Green's function $G_{xr}\ (r, \theta = 0, z)$ and vertical component $G_{zz}\ (r, \theta = 0, z)$, respectively. The results are shown in Figs. 12, 13 and 14. In the figures, $\bar{\omega}$ is the normalized frequency, $\bar{\omega} = a_0 r = \omega r\sqrt{\rho_0/d_{66}^0}$. Generally, it can be observed from Figs. 12, 13 and 14 that the dynamic response induced by the external excitations strongly depends on the degree of material anisotropy. In detail, the

increase in the ratios $\bar{E}/\bar{E}'$ and $\bar{G}/\bar{G}'$ does have a great influence on the horizontal and vertical displacement. It reflects the fact that the displacement increases with the rise of deformability in the direction parallel to the applied load. Also, with increasing $\bar{E}/\bar{E}'$ and $\bar{G}/\bar{G}'$, the peaks of both the horizontal and vertical displacement shift to the side of lower frequency. The change in ν/ν' does not significantly shift the peaks of the horizontal and vertical displacement; the tendency of the curves is almost identical. However, it stresses an important influence on the amplitude of the displacement. Additionally, it is interesting to note that the horizontal and vertical displacements are less affected by the value of ν/ν' at the lower frequency range.

7 Conclusions

In this paper, a numerical approach is proposed for the calculation of Green's function for a transversely isotropic multi-layered half-space. The whole algorithm is unconditionally stable and retains the computational simplicity with only the algebraic calculations involved. It imposes no limit to the thickness of the layered medium and the magnitude of frequency. In the analysis, it employs the domain transformation, dual vector representation of wave motion equation and precise integration method. In the numerical implementation, the Fourier–Bessel transform is employed to transform the wave motion equation from spatial domain to wavenumber domain, which results in a set of second-order ordinary differential equations. The dual vector representation of wave motion equation is introduced to reduce the second-order differential equation to first order. Then, the precise integration method is used to solve it. Finally, the Green's function in the wavenumber domain is obtained. To obtain the Green's function in the spatial domain, the inverse Fourier–Bessel transform over wavenumber is conducted, which gives a one-dimensional infinite integral with Bessel functions involved. In order to perform the infinite integrals, an adaptive Gauss quadrature is used. Numerical examples are provided. Comparisons have been made with the results available in the literature. Very good agreement is reached. Also, it investigated the Green's function for a transversely isotropic five-layered semi-infinite space and illustrated the effect of the material anisotropy. To analyze the multi-layered half-space, the proposed approach has the following advantages: the dual vector form of matrices makes the combinations of two adjacent sub-/mini-layers into a new jointed sub-/mini-layer quite easy. Since the dimension of the matrices is 3×3, partitioning each layer into a large number of mini-layers and employing the precise integration method, the calculation is computationally stable and efficient. It enables higher accuracy of the results to be achieved.

Acknowledgments The financial support from the Siemens AG and DAAD (German Academic Exchange Service) for the author is gratefully acknowledged.

References

1. Ward, W., Marsland, A., Samuels, S.: Properties of the London clay at the Ashford common shaft: in-situ and undrained strength tests. Geotechnique **15**, 321–344 (1965)
2. Atkinson, J.: Anisotropic elastic deformations in laboratory tests on undisturbed London clay. Geotechnique **25**, 357–374 (1975)
3. Abelev, A.V., Lade, P.V.: Effects of cross anisotropy on three-dimensional behavior of sand. I: stress–strain behavior and shear banding. J. Eng. Mech. **129**, 160–166 (2003)
4. Singh, B.: Wave propagation in a prestressed piezoelectric half-space. Acta Mech. **211**, 337–344 (2010)
5. Zheng, P., Zhao, S.-X., Ding, D.: Dynamic Green's functions for a poroelastic half-space. Acta Mech. **224**, 17–39 (2013)
6. Zheng, P., Ding, B., Zhao, S.X., Ding, D.: Dynamic response of a multilayered poroelastic half-space to harmonic surface tractions. Transp. Porous Media **99**, 229–249 (2013)
7. Stoneley, R.: The seismological implications of aeolotropy in continental structure. Geophys. Suppl. Mon. Notices R. Astron. Soc. **5**, 343–353 (1949)
8. Anderson, D.L.: Elastic wave propagation in layered anisotropic media. J. Geophys. Res. **66**, 2953–2963 (1961)
9. Buchwald, V.: Rayleigh waves in transversely isotropic media. Q. J. Mech. Appl. Math. **14**, 293–318 (1961)
10. Singh, S.J.: Static deformation of a transversely isotropic multilayered half-space by surface loads. Phys. Earth Planet. Inter. **42**, 263–273 (1986)
11. Seale, S.H., Kausel, E.: Point loads in cross-anisotropic, layered halfspaces. J. Eng. Mech. **115**, 509–524 (1989)
12. Rajapakse, R., Wang, Y.: Green's functions for transversely isotropic elastic half space. J. Eng. Mech. **119**, 1724–1746 (1993)
13. Wang, C.D., Tzeng, C.S., Pan, E., Liao, J.J.: Displacements and stresses due to a vertical point load in an inhomogeneous transversely isotropic half-space. Int. J. Rock Mech. Min. Sci. **40**, 667–685 (2003)
14. Wang, X., Shen, Y.-P.: The general solution of three-dimensional problems in magneto electroelastic media. Int. J. Eng. Sci. **40**, 1069–1080 (2002)

15. Shodja, H.M., Eskandari, M.: Axisymmetric time-harmonic response of a transversely isotropic substrate–coating system. Int. J. Eng. Sci. **45**, 272–287 (2007)
16. Rahimian, M., Eskandari-Ghadi, M., Pak, R.Y., Khojasteh, A.: Elastodynamic potential method for transversely isotropic solid. J. Eng. Mech. **133**, 1134–1145 (2007)
17. Pao, Y.-H.: Elastic waves in solids. J. Appl. Mech. **50**, 1152–1164 (1983)
18. Nayfeh, A.H.: Wave Propagation in Layered Anisotropic Media: With Application to Composites. Elsevier, Amsterdam (1995)
19. Vanderhijden, J.H.M.T.: Propagation of Transient Elastic Waves in Stratified Anisotropic Media. Amsterdam, North-Holland (1987)
20. Tan, E.L.: A robust formulation of SAW Green's functions for arbitrarily thick multilayers at high frequencies. IEEE Trans. Ultrasonics Ferroelectr. Freq. Control **49**, 929–936 (2002)
21. Tan, E.L.: Matrix algorithms for modeling acoustic waves in piezoelectric multilayers. IEEE Trans. Ultrasonics Ferroelectr. Freq. Control **54**, 2016–2023 (2007)
22. Pan, E., Bevis, M., Han, F., Zhou, H., Zhu, R.: Surface deformation due to loading of a layered elastic half-space: a rapid numerical kernel based on a circular loading element. Geophys. J. Int. **171**, 11–24 (2007)
23. Pan, E., Han, F.: Green's functions for transversely isotropic piezoelectric multilayered half-spaces. J. Eng. Math. **49**, 271–288 (2004)
24. Khojasteh, A., Rahimian, M., Eskandari, M., Pak, R.Y.S.: Asymmetric wave propagation in a transversely isotropic half-space in displacement potentials. Int. J. Eng. Sci. **46**, 690–710 (2008)
25. Khojasteh, A., Rahimian, M., Eskandari, M., Pak, R.Y.S.: Three-dimensional dynamic Green's functions for a multilayered transversely isotropic half-space. Int. J. Solids Struct. **48**, 1349–1361 (2011)
26. Waas, G., Riggs, H., Werkle, H.: Displacement solutions for dynamic loads in transversely-isotropic stratified media. Earthq. Eng. Struct. Dyn. **13**, 173–193 (1985)
27. Kausel, E.: Wave propagation in anisotropic layered media. Int. J. Numer. Methods Eng. **23**, 1567–1578 (1986)
28. Oliveira Barbosa, J.M., Kausel, E.: The thin-layer method in a cross-anisotropic 3D space. Int. J. Numer. Methods Eng. **89**, 537–560 (2012)
29. Zhong, W.-X.: On precise integration method. J. Comput. Appl. Math. **163**, 59–78 (2004)
30. Zhong, W., Zhu, J., Zhong, X.-X.: On a new time integration method for solving time dependent partial differential equations. Comput. Methods Appl. Mech. Eng. **130**, 163–178 (1996)
31. Zhong, W.: Combined method for the solution of asymmetric Riccati differential equations. Comput. Methods Appl. Mech. Eng. **191**, 93–102 (2001)
32. Zhang, J., Gao, Q., Tan, S.J., Zhong, W.X.: A precise integration method for solving coupled vehicle–track dynamics with nonlinear wheel–rail contact. J. Sound Vib. **331**, 4763–4773 (2012)
33. Zhong, W.X., Lin, J., Gao, Q.: The precise computation for wave propagation in stratified materials. Int. J. Numer. Methods Eng. **60**, 11–25 (2004)
34. Gao, Q., Lin, J.H., Zhong, W.X., Howson, W.P. Williams F.W.: A precise numerical method for Rayleigh waves in a stratified half space. Int. J. Numer. Methods Eng. **67**, 771–786 (2006)
35. Lin, G., Han, Z., Li, J.: An efficient approach for dynamic impedance of surface footing on layered half-space. Soil Dyn. Earthq. Eng. **49**, 39–51 (2013)
36. Lin, G., Han, Z., Zhong, H., Li, J.: A precise integration approach for dynamic impedance of rigid strip footing on arbitrary anisotropic layered half-space. Soil Dyn. Earthq. Eng. **49**, 96–108 (2013)
37. Lin, G., Han, Z., Li, J.: Soil–structure interaction analysis on anisotropic stratified medium. Géotechnique **64**, 570–580 (2014)
38. Lin, G., Han, Z., Li, J.: General formulation and solution procedure for harmonic response of rigid foundation on isotropic as well as anisotropic multilayered half-space. Soil Dyn. Earthq. Eng. **70**, 48–59 (2015)
39. Singh, V.K., Singh, O.P., Pandey, R.K.: Numerical evaluation of the Hankel transform by using linear Legendre multi-wavelets. Comput. Phys. Commun. **179**, 424–429 (2008)
40. Singh, V.K., Pandey, R.K., Singh, S.: A stable algorithm for Hankel transforms using hybrid of block-pulse and Legendre polynomials. Comput. Phys. Commun. **181**, 1–10 (2010)
41. Han, Z., Lin, G., Li, J.: Dynamic impedance functions for arbitrary-shaped rigid foundation embedded in anisotropic multilayered soil. J. Eng. Mech. 04015045 (2015). doi:10.1061/(ASCE)EM.1943-7889.0000915
42. Kausel, E.: Fundamental Solutions in Elastodynamics: A Compendium. Cambridge University Press, Cambridge (2006)
43. Chave, A.D.: Numerical integration of related Hankel transforms by quadrature and continued fraction expansion. Geophysics **48**, 1671–1686 (1983)
44. Lucas, S.K.: Evaluating infinite integrals involving products of Bessel functions of arbitrary order. J. Comput. Appl. Math. **64**, 269–282 (1995)
45. Kausel, E., Peek, R.: Dynamic loads in the interior of a layered stratum: an explicit solution. Bull. Seismol. Soc. Am. **72**, 1459–1481 (1982)
46. Kausel, E.: An explicit solution for the Green functions for dynamic loads in layered media. Research Report R81-13, Publication No. 699, Dept. of Civil Engineering, M.I.T., Cambridge, MA
47. Rokhlin, S., Wang, L.: Stable recursive algorithm for elastic wave propagation in layered anisotropic media: stiffness matrix method. J. Acoust. Soc. Am. **112**, 822–834 (2002)
48. Horn, R.A., Johnson, C.R.: Matrix Analysis. Cambridge University Press, Cambridge (2012)
49. Chen, L.: Dynamic interaction between rigid surface foundations on multi-layered half space. Int. J. Struct. Stabil. Dyn. 1550004 (2015). doi:10.1142/S0219455415500042
50. Park, J.: Wave Motion in Finite and Infinite Media Using the Thin-Layer Method. Massachusetts Institute of Technology, Cambridge (2002)